ORIGINAL ARTICLE
Journal Section

Structural Development of Speech Networks in Young Children at Risk for Speech Disorder

Marilyn Curtis[1] | Mohammadreza Bayat[1] | Dea Garic[2] | Alliete R. Alfano[1] | Melissa Hernandez[1] | Madeline Curzon[1] | Andrea Bejarano[1] | Pascale Tremblay[3] | Paulo Graziano[1] | Anthony Steven Dick[1]

[1]Department of Psychology and the Center for Children and Families, Florida International University, Miami, Florida, 33199, United States

[2]University of North Carolina at Chapel Hill, Carolina Institute for Developmental Disabilities, Chapel Hill, NC, 27599, United States

[3]Université Laval, Department of Rehabilitation Sciences, Quebec City, Quebec, Canada

Correspondence
Anthony Steven Dick PhD, Department of Psychology and the Center for Children and Families, Florida International University, Miami, Florida, 33199, United States
Email: adick@fiu.edu

Funding information
Funding from National Institutes of Health, Grant/Award Numbers: R01MH112588, R01DK119814, R56MH108616.

Characterizing the structural development of the neural speech network in early childhood is important for understanding speech acquisition. To investigate speech in the developing brain, 94 children aged 4-7-years-old at risk for early speech disorder were scanned using diffusion weighted imaging (DWI) magnetic resonance imaging (MRI). Additionally, each child completed the Syllable Repetition Task (SRT), a validated measure of phoneme articulation. The DWI data were modeled using multi-compartment restriction spectrum imaging (RSI) to measure restricted and hindered diffusion properties in both grey and white matter. Consequently, we analyzed the diffusion data using both whole brain analysis, and automated fiber quantification (AFQ) analysis to establish tract profiles for each of six fiber pathways thought to be important for supporting speech development. In the whole brain analysis, we found that SRT performance was associated with restricted diffusion in bilateral inferior frontal gyrus (*pars opercularis*), right pre-supplementary/supplementary motor area (pre-SMA/SMA), and bilateral

Abbreviations: ADHD, Attention-Deficit/Hyperactivity Disorder

cerebellar grey matter ($p < .005$). Age moderated these associations in left *pars opercularis* and frontal aslant tract (FAT). However, in both cases only the cerebellar findings survived a cluster correction. We also found associations between SRT performance and restricted diffusion in cortical association fiber pathways, especially left FAT, and in the cerebellar peduncles. Analyses using automatic fiber quantification (AFQ) highlighted differences in high and low performing children along specific tract profiles, most notably in left but not right FAT. These findings suggest that individual differences in speech performance are reflected in structural gray and white matter differences as measured by restricted and hindered diffusion metrics, and offer important insights into developing brain networks supporting speech in very young children.

KEYWORDS
Diffusion-Weighted Imaging, Speech, Frontal Aslant Tract, Development, Cerebellum, Inferior Frontal Gyrus, Restriction Spectrum Imaging

1 | INTRODUCTION

Contemporary neurobiological models of speech have clarified the primary brain regions and connections that are putatively important for speech. Such models developed in adults are potentially relevant for understanding developing speech in young children, an understudied population with regard to the neurobiology of speech. In fact, very little is known about the development of neural speech pathways in early childhood (although see (Broce et al., 2015; S.-E. Chang et al., 2015; Johnson et al., 2022). This highlights a major deficit in our knowledge of the neurobiology of speech development. The neurobiological models based in adults allow for some expectation about which brain regions and fiber pathways might be sensitive to individual differences in speech ability as children develop in this age range, but this remains untested. With an understanding of how speech develops in the brain, we can build better developmental models relevant for understanding early disorders of speech perception and production.

The two pertinent contemporary models of speech neurobiology that will frame this investigation–Guenther's GODIVA model (Guenther, 2016) and Hickok's updated model (Hickok et al., 2023) –describe how speech can be construed as a broad, distributed network that includes subcortical and cortical structures, and the white matter pathways which connect them (see Figure 1 for an overview of relevant structures and pathways). According to Guenther, the neural speech network can be parsed into bilateral cortical and subcortical information loops that shape the motor cortical commands for speech (Guenther, 2016). The cortico-basal ganglia loop connects basal ganglia structures (globus pallidus, substantia nigra, caudate, and the putamen), and the ventral lateral nucleus of the thalamus, with various regions of the cerebral cortex, such as the supplementary motor area (SMA) and pre-SMA, the primary motor

cortex, the somatosensory cortex, and the premotor cortex (Guenther, 2016). The information loop connecting these subcortical structures plays a key role in the process of selecting and initiating appropriate motor programs for speech (Guenther, 2016). The cortico-cerebellar loop, consisting of projections through the pons, deep cerebellar nuclei, the thalamus, and the cerebral cortex, is crucial in the generation of finely timed muscle activations necessary for rapid speech production (Guenther, 2016). The information loops described provide a direct pathway connecting the subcortical structures with the cerebral cortex, where somatosensory and motor representations are integrated, and the motor commands necessary for speech production are generated and initiated.

An extensive cortical model is also presented by Hickok and colleagues (Hickok et al., 2023). They postulate a model of speech coordination across dual processing streams which integrates primary motor cortical regions, precentral speech areas with prominent roles in speech coordination, and multiple cortical regions necessary for speech production and perception, such as the inferior frontal gyrus (IFG) and superior temporal sulcus (STS). According to this model, speech can be construed as a distributed network across two broad processing streams: the ventral stream, which maps sound onto meaning, and the dorsal stream, which maps sound onto articulatory-based representations (Hickok & Poeppel, 2000, 2004, 2007). The left-dominant dorsal stream has a sensorimotor interface between parietal and temporal regions which projects to an articulatory network in the frontal lobe supporting articulation, specifically involving the posterior IFG (namely *pars opercularis*), the premotor cortex, and the anterior insula (Hickok & Poeppel, 2007). The bilaterally-organized ventral stream is a combinatorial lexical interface implicated in speech recognition, which connects the anterior and posterior regions of the middle temporal gyrus (MTG) and inferior temporal sulcus (ITS) (Hickok & Poeppel, 2007), extending beyond the classic left-hemisphere dominant model of speech (Tremblay & Dick, 2016). Evidence from neuroimaging studies have demonstrated an overlap in speech perception and speech production within the superior temporal gyrus (STG), incorporated in both streams (Buchsbaum et al., 2001; Hickok et al., 2003). The dual-stream model expands more simplistic models which envision speech as communication between separate regions controlling speech production and speech perception.

The contributions of the left IFG, neighboring frontal operculum, and insular cortex are emphasized by both Guenther and Hickok and colleagues. Although not addressed in Hickok and colleagues, Guenther additionally emphasizes medial frontal regions associated with motor planning, such as the pre-SMA and SMA. These regions are supported by a monosynaptic pathway known as the frontal aslant tract (Figure 2). The FAT's connectivity of the IFG and pre-SMA/SMA, regions previously associated with motor speech properties (Hertrich et al., 2016), suggests that it may play a role in planning and initiation of speech, especially in the left hemisphere (Dick et al., 2019). Several studies have demonstrated the FAT's association with various aspects of speech, specifically verbal fluency (Catani et al., 2013; Mandelli et al., 2014), motor speech initiation (Kinoshita et al., 2015; Zhong et al., 2022a), speech fluency impairments such as stuttering (Kemerdere et al., 2016; Kronfeld-Duenias et al., 2016; Misaghi et al., 2018), and speaking rate (Jossinger et al., 2023). Few studies have explored the development of the FAT in young children. For example, Broce and colleagues (Broce et al., 2015) tracked the FAT in young children (5-8-year-olds), but found no associations with phonology and expressive language. One study has linked FAT diffusion properties to stuttering in 6-12-year-old children (Misaghi et al., 2018). However, no studies, to our knowledge, have examined developmental variability of the FAT in relation to speech in very young children, as we propose to do here.

The left IFG is also a key node in a dorsal pathway for speech (Hickok et al., 2003; Hickok & Poeppel, 2004, 2007; Rauschecker, 1998; Rauschecker & Scott, 2009) mapping sounds onto articulatory-based representations through interactions with the posterior STG and STS (STGp and STSp), planum temporale, and supramarginal gyrus. The structural connectivity of these regions has been established via several invasive and non-invasive methods (Bernard et al., 2019; Willems et al., 2009). Two major fiber pathways are thought to support dorsal stream connectivity–the superior

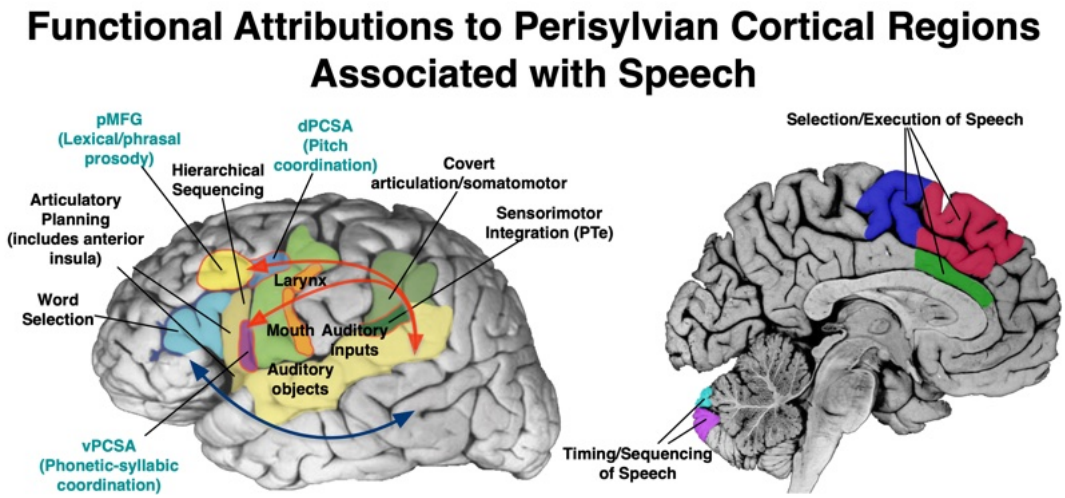

FIGURE 1 Cortical regions supporting speech are examined in the current study, situated within a broader bilateral but strongly left-lateralized perisylvian language network. The dorsal stream (upper red arrows) is primarily proposed to support sensorimotor speech processing via posterior superior temporal gyrus and sulcus, *planum temporale* (PTe), and inferior parietal regions (supramarginal gyrus), connecting to inferior frontal and more dorsal premotor regions. Connectivity to pre-supplementary and supplementary motor areas (medial regions in red and blue), basal ganglia (not shown), and cerebellum, rounds out a distributed system supporting speech. The ventral stream (blue arrow) regions primarily support lexial and semantic processing at word, sentence and narrative levels.

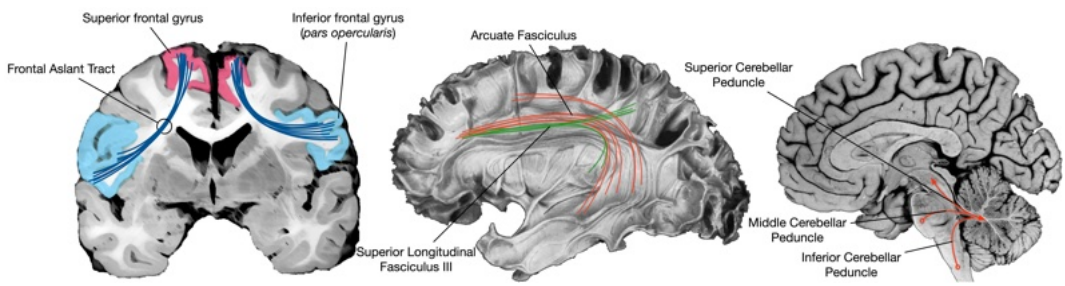

FIGURE 2 Cortical and cerebellar pathways supporting speech are examined in the current study. The frontal aslant tract (FAT) connects inferior frontal gyrus and pre-supplementary motor area; superior longitudinal fasciculus III and arcuate fasciculus connect inferior frontal and dorsal premotor cortex with supramarginal gyrus and superior and middle temporal cortex; the three brainstem peduncles support communication with cerebellum.

longitudinal fasciculus III (SLF III) and the arcuate fasciculus (AF). SLFIII is thought to support a fronto-parietal articulatory loop implicated in motor speech function, based on disturbances during electrostimulation (Duffau et al., 2003). SLF III is specifically defined by its connectivity with the supramarginal gyrus, involved in processing phonological inputs and outputs (Oberhuber et al., 2016), and IFG and frontal operculum (Bernal & Altman, 2009), thus establishing its putative role in both speech perception and production. AF projects more broadly, connecting posterior temporal and inferior parietal cortex with both ventral and superior frontal cortical regions (Barbeau et al., 2020). It has been proposed that the AF plays a role in speech monitoring and motor speech function, due to established connectivity

with premotor and primary motor areas in the precentral gyrus (Bernal & Ardila, 2009). Hickok and colleagues have recently delineated a region possibly facilitated by this connectivity, referred to as the dorsal precentral speech area (Hickok et al., 2023). This area has been demonstrated to exert significant influence over prosodic control, an element of speech production. Supporting the assertion that the SLF and AF play a role in speech perception and production is a study that demonstrated an association with the AF and associated segments, including the SLF III, and receptive and expressive language in 5-8-year-old children (Broce et al., 2015). The proposed study seeks to expand on previous research implicating the AF and SLF III in developmental speech and language abilities by focusing on a specific component of speech, phoneme articulation, which will allow us to further parse the specific functions of these support pathways.

The cerebellum and its associated connectivity are also known to support speech and potentially speech development (Jobson et al., 2022). The involvement of the cerebellum in verbal fluency and articulation tasks is well-established (Riecker et al., 2006; Riecker et al., 2005; Schlösser et al., 1998), and anatomical evidence of functional connectivity suggests that the role of the cerebellum may go beyond simple motor generation and activation, as previously thought. As reviewed in Vias and Dick (Vias & Dick, 2017), lateral and medial regions of cerebellar grey matter have been associated with distinct aspects of speech perception and production. Two of the cerebellar lobules that fall along the horizontal cerebellar fissure, Crus I and Crus II, have been shown to play a role in phonological processing through word generation and phonemic and verb fluency tasks (Frings et al., 2006; Schweizer et al., 2010; Stoodley et al., 2012). Activation during fMRI tasks of speech production have revealed bilateral findings in the Crus I and Crus II lobules in adults, but little is known about the development of these regions in very young children with regard to speech (Bohland & Guenther, 2006; Correia et al., 2020; Geva et al., 2021; Peeva et al., 2010; Shuster & Lemieux, 2005). The inferior, middle, and superior cerebellar peduncles (ICP, MCP, and SCP) are the three major white matter input and output pathways of the cerebellum (Naidich et al., 2009), linking the lateral cerebellar cortex with subcortical and cortical structures in the cerebral cortex (Vias & Dick, 2017). The right ICP has been linked to developmental differences in children who stutter (Johnson et al., 2022), and in adults with developmental stuttering, speech rate has been associated with white matter cellular properties of the left ICP (Jossinger et al., 2021). Additionally, white matter properties of the ICP have been correlated with articulation rate, one facet of speech production (Jossinger et al., 2021; Jossinger et al., 2023; Kronfeld-Duenias et al., 2016). In neurotypical adults, the right SCP has been associated with semantic and phonemic verbal fluency, while the right MCP is associated with speaking rate (Jossinger et al., 2023), demonstrating that these distinct cerebellar pathways contribute to elements of speech production beyond articulatory control, such as lexical access (Jossinger et al., 2023). The cerebellum has also been implicated in fine speech control during childhood for children with early speech deficits (A. Morgan et al., 2011). However, the precise anatomical structures and functional connectivity contributing to such deficits are still unknown. While the cerebellar peduncles and cerebellar grey matter have been established in aspects of speech production and perception, further research is necessary to probe how the connectivity of cerebellar regions is integrated within the broader cortical speech network during development.

1.1 | Measurement of white matter properties in the developing brain

To explore development of the neural regions and connectivity supporting speech, we focused on structural development as measured by diffusion-weighted imaging (DWI). Traditionally, DWI studies have exclusively contributed to understanding white matter development in specific fiber pathways, or in white matter defined broadly (e.g., via analysis of tract-based spatial statistics). These approaches generally focus on the measurement of anisotropic diffu-

sion within axons, typically using diffusion-tensor or higher-order spherical deconvolution models. For example, most studies conducting tractography examine fractional anisotropy (FA) differences across age, or in association with individual differences in performance on some task. In contrast, in this study we explored a novel diffusion analysis method called restriction spectrum imaging (RSI), which is a multi-compartment model of the diffusion signal. This model quantifies the relative proportion of restricted, hindered, and free water diffusion in each voxel of tissue in the brain (Palmer et al., 2022a). The novelty of RSI is that we can measure both white matter tracts and grey matter of the cortex, subcortical structures, and cerebellum (Palmer et al., 2022a). The normalized total signal fractions for restricted (RNT) and hindered (HNT) diffusion produced by this method can be interpreted as reflecting the relative contributions of maturational and developmental cellular processes associated with cell bodies and neurites to diffusion signal in the different compartments. Thus, we can measure the relationship between RSI metrics and cellular processes in both grey and white matter structures of the speech network that can be related to individual behavioral differences.

With RSI, we can examine individual differences in both grey and white matter. However, we can also apply more sophisticated analysis to the white matter tracts themselves. We do this here with Automated Fiber Quantification (AFQ)(Yeatman et al., 2012). Unlike traditional tractography methods that average across the entire white matter bundle, AFQ segements each tract into 100 equidistant nodes, allowing us to establish a "tract profile" for each child and observe individual differences at specific positions along the tracts (Yeatman et al., 2012), and how these individual differences are associated with behavior. For the current analysis, we were interested in white matter pathways associated with the neural speech network, specifically the FAT, AF, SLF III, and superior, middle, and inferior cerebellar peduncles (SCP, MCP, ICP). It is anticipated that these pathways will display differences in measured restricted and hindered diffusion values along the white matter tracts based on speech performance measured by a phoneme articulation task.

1.2 | Variability of speech production in developmental samples at risk for speech delay or disorder

Examining individual differences in speech production and its association with structural development requires substantial variability in both microstructural properties of the brain, and performance on a behavioral task. In order to expand the degree of variability in speech performance, we included as part of the typically developing (TD) sample a sample of children diagnosed with attention-deficit/hyperactivity disorder (ADHD). The reason for the inclusion of this sample of children was two-fold. First, it was a practical choice given our data collection of the TD sample was part of a broader study that included children with ADHD. Scientifically, we leverage the inclusion of children with ADHD because they are at high risk of comorbid speech delay (McGrath et al., 2008), and thus are more likely to display a high degree of variability in speech performance. Although the percentages vary, clinical studies have suggested that between 40%-64% of children diagnosed with ADHD have speech and language difficulties requiring evaluation and/or therapeutic intervention (Humphries et al., 1994; Taylor, 1991). The broader performance distribution observed among a sample of children with ADHD compared to TD children offers a distinct and valuable backdrop for delineating the developmental trajectories of various brain regions and fiber pathways implicated in speech.

1.3 | The Present Study

In summary, the primary aim of the present study is to probe how the neural systems implementing speech develop structurally in children with a wide variety of speech production abilities, including children at-risk for speech disorders, such as those with ADHD. A validated measure of phoneme articulation known as the Syllable Repetition Task (SRT) was used to explore the specific role of these regions of interest (ROIs). We predict that 1) performance on the SRT will be associated with grey matter celluarity in the cortical and subcortical regions identified to be involved in the neural network of speech; 2) these associations will be moderated by age; and 3) performance on the SRT will be associated with white matter microstructural properties in the fiber pathways involved with speech perception and speech production, including the FAT, AF, SLF III, and the three cerebellar peduncles.

2 | METHOD

2.1 | Participants

This study is a substudy of a broader research project examining 322 4-7-year-olds. That study involved MRI scanning and collection of various behavioral and clinical measures. Roughly half of that broader study sample had a diagnosis of ADHD. For this substudy, 113 children also completed the SRT outside the MRI scanner (the COVID pandemic prohibited continued data collection of this particular measure on the full sample because the head-mounted microphone was a transmission risk). We focus in this substudy on the sample of 113 participants who completed the task.
Of the 113 participants who completed the SRT, 19 participants were excluded based on excessive movement (see Image Acquisition below) and/or the fact that they were left-handed (defined by the Edinburgh Handedness Inventory) (Oldfield, 1971). Thus, the final analyzed sample size was n = 94 (M_{age} = 5.5 years, SD = 0.82, 70 males).

Recruitment and Eligibility Requirements. The study took place in a large urban southeastern city in the U.S. with a large Hispanic/Latino population. Children and their caregivers were recruited from local schools, open houses/parent workshops, mental health agencies, and radio and newspaper ads. Exclusionary criteria for the children included intellectual disability (IQ lower than 70 on the Wechsler Preschool and Primary Scale of Intelligence 4th edition; WPPSI-IV), confirmed history of Autism Spectrum Disorder, and currently or previously taking psychotropic medication.

Demographics of the Sample. Within this sub-sample, there were 47 typically-developing children and 47 children who were diagnosed with ADHD. ADHD diagnosis was accomplished through a combination of parent structured interview (C-DISC (Shaffer et al., 2000) and parent and teacher ratings of symptoms and impairment (Disruptive Behavior Disorders Rating Scale (DBD), which involves teacher and parent reporting of symptoms (Fabiano et al., 2006a; Graziano et al., 2022), and Impairment Rating Scales (Fabiano et al., 2006b). For this study, ADHD was not considered categorically, but we controlled for ADHD symptoms of inattention and hyperactivity, as measured by the DBD.

The demographic breakdown of the subsample was: 82% Hispanic/Latino; 87% White; 7% Black; 3% Asian; 3% More than one race. The distribution of maternal education in AHEAD also suggests a good range in our sample catchment: 8.6% of mothers had a high school degree or less, 15.2% had some college, 13.0% had associates degrees, 25.0% had bachelor's degrees, and 38.0% had an advanced degree.

2.2 | Experimental Paradigm

Children completed an MRI scan and the SRT on the same day, as described below.

Syllable Repetition Task (SRT). The SRT is a child-friendly speech task that examines expressive speech abilities in individuals with limited phonetic inventories, such as young speakers (Shriberg & Lohmeier, 2008). Research suggests that the SRT is an accurate and stable task for measuring expressive language impairment, as well as auditory-perceptual speech processing errors (Shriberg et al., 2009). The task measures prearticulatory planning and subsequent planning of articulatory gestures prior to motor execution of speech, which includes prearticulatory encoding and memory of speech sounds, phonological planning, and transforming the phonological plan into a motor plan (Levelt et al., 1999; Rvachew & Matthews, 2017).

During the task, children were asked to repeat a list of 18 two-to four-syllable nonsense words which were played over computer speakers. The task is available as part of a power-point presentation with the audio embedded in each slide, which includes text. The experimenter ensured that the slide presentation was turned away from the participant so that children who could read did not use orthographic information to complete the task. The task starts with simple, two-syllable nonwords such as "ba-da", and increases in difficulty to nonwords such as "ba-na-ma-da". Children were recorded during the task with a head-mounted microphone.

The recordings were independently transcribed and scored by three Spanish-English bilingual research assistants and scored according to the SRT scoring manual, which provided a final percentage score for proportion of correct syllables spoken. Syllable additions, or syllables that the participant produced that were not part of the target word, were tallied. If four or more responses included syllable additions (25% of items), the score was deemed invalid. In addition, given the large proportion of bilingual Spanish/English speaking children enrolled in our study and since the SRT was developed for monolingual English-speaking participants, we decided to score the SRT using both the traditional scoring manual as well as a modified bilingual scoring system. The bilingual scoring method modified the traditional scoring method to allow for b/v substitutions, which are two separate phonemes in English but are commonly both pronounced as "b" in Spanish.

Three transcribers, all Spanish-English bilinguals, were trained by a licensed Spanish-English bilingual speech-language pathologist (author A.R.A.). The three transcribers scored according to the blingual scoring method and had a moderate inter-rater reliability score of κ = 0.587 (Cohen, 1960). In cases of disagreement, the score for each word was determined by majority (2 out of 3) vote. If agreement could not be reached, the recording was replayed with all transcribers and a licensed Spanish-English bilingual speech-language pathologist present for a final determination. The bilingual scoring was used in the present analysis.

The sample provided a good range of scores on the SRT, providing sufficient variability to examine associations with our brain measures. Performance on the percent correct syllables ranged from 22 to 100, with a mean percentage of 83.67% (SD = 14.14; see Figure 3). We also examined if there were performance differences between children diagnosed with ADHD and typically developing children. There was not a significant difference in performance between the groups $t(92) = -1.20$, $p = 0.23$, so we did not examine group in the analysis. Instead, as described below, we controlled for inattention and hyperactivity symptoms.

2.3 | Image Acquisition

All imaging was performed using a research-dedicated 3-T Siemens MAGNETOM Prisma MRI scanner (V11C) with a 32-channel coil located on the university campus. Children first completed a preparatory phase using realistic mock scanner in the room across the hall from the magnet. Here, they were trained to stay still and were also acclimated to the enclosed space of the magnet, to the back projection visual presentation system and to the scanner noises (in

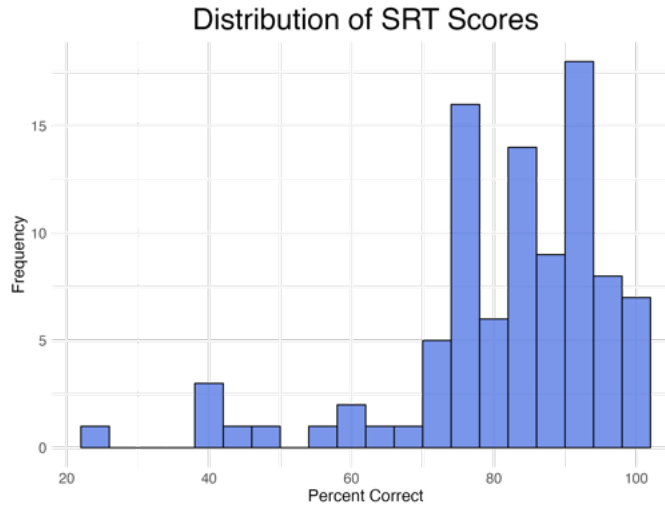

FIGURE 3 A histogram of performance on the Syllable Repetition Task (SRT) displays scores as the percentage correct, as measured by the bilingual scoring system. The figure shows a good range of performance, with some degree of negative skew.

this case, presented with headphones). When they were properly trained and acclimated, they were moved to the magnet. In the magnet, during the structural scans, children watched a child-friendly movie of their choice. Sound was presented through MRI-compatible headphones that also functioned as additional ear protection.

T1-weighted and DWI scans were acquired for each participant. T1-weighted MRI scans were collected using a 3D T1-weighted inversion prepared RF-spoiled gradient echo sequence (axial; TR/TE 2500/2.88; 1 x 1 x 1 mm, 7 min 12 s acquisition time) with prospective motion correction (Siemens vNav; (Tisdall et al., 2012)), according to the Adolescent Brain Cognitive Development (ABCD) protocol (Hagler Jr et al., 2019).

Movement artifacts pose challenges for T1-weighted images, impacting registration to the diffusion scan. Each T1 image underwent thorough inspection by A.S.D. We applied a visual rating system ranging from 'poor = 1' to 'excellent = 4' was employed for each T1-weighted image, with half-point allowances (e.g., 3.5). Most images were in the 3-4 range, with an average image rating of 3.63 (*SD* = 0.53)

DWI scans were acquired via high-angular-resolution diffusion imaging (HARDI) with multiband acceleration factor 3 (EPI acquisition; TR/TE = 4100/88 ms; 1.7 x 1.7 x 1.7 mm; 81 slices no gap; 96 diffusion directions plus 6 b = 0 s/mm^2: b = 0 [6 dirs], b = 500 [6-dirs], 1000 [15-dirs], 2000 [15-dirs] and 3000 [60-dirs] s/mm^2; A-to-P direction [7 m 31 s acquisition time]). A second brief scan at b = 0 s/mm^2 in P-to-A direction was acquired to help deal with susceptibility artifacts.

Image Post-Processing. DWI preprocessing was performed using a number of complementary software suites. The steps were as follows: 1) outlier detection and replacement, and volume-to-slice correction using a synthetized DWI model, implemented in FSL eddy (Andersson et al., 2017; Andersson et al., 2016) (note motion and eddy current distortion correction are implemented in the next step); 2) motion and eddy-current distortion correction, implemented with TORTOISE DIFFPREP (Barnett et al., n.d.) instead of FSL eddy; 3) creation of a synthesized T2-weighted image from the T1-weighted scan using Synb0-DisCo (Schilling et al., 2020; Schilling et al., 2019); 4) correction of spatial

and intensity distortions caused by B_0 field inhomogeneity, using TORTOISE DRBUDDI (Irfanoglu et al., 2015) implementing blip-up/blip-down distortion correction (Andersson et al., 2003; H. Chang & Fitzpatrick, 1992; D. Holland et al., 2010; P. S. Morgan et al., 2004). This step uses both the reverse-phase encoded b = 0 s/mm^2 image for the estimation of the field map, and the synthesized T2-weighted image for imposition of geometry constraints; 5) gradient non-linearity correction (gradwarp) using the gradient coefficients supplied by Siemens (Bammer et al., 2003; Barnett et al., 2021; Glover & Pelc, 2019). The outlier-replaced, slice-to-volume registered, transformed for motion, eddy-current corrected, b0-induced susceptibility field corrected, gradient non-linearity corrected images are resampled to the T1-weighted resolution (to 1 mm^3) and registered to the T1-weighted image in a single interpolation step.

2.4 | Diffusion Metrics

Restriction Spectrum Imaging. We took advantage of the multi-shell HARDI acquisition to implement a reconstruction of the diffusion signal with the RSI model (Brunsing et al., 2017; White, Leergaard, et al., 2013a; White, McDonald, Farid, et al., 2013; White et al., 2014). The RSI model can be used to quantify the relative proportion of restricted, hindered, and free water diffusion within each voxel of the brain. These components–restricted, hindered, and free water–have intrinsic diffusion characteristics. Free water (e.g., cerebrospinal fluid) is water diffusion unimpeded by tissue structure. In biological tissue, though, the two additional modes of hindered and restricted diffusion predominate (Bihan, 1995). Hindered diffusion describes the behavior of water hindered by the presences of neurites, glia, and other cells, and follows a Guassian displacement pattern. The signal originates from both extracellular and intracellular spaces with dimensions larger than the diffusion length scale (10 μ m), and it is affected by the diffusion path length that molecules must travel to navigate cellular obstructions. On the other hand, the primary source of restricted diffusion signal in biological tissue comes from cell membranes. Restricted diffusion thus relates to the physical obstruction of molecules within cellular compartments. If the diffusion time Δ is long enough, the length scale of diffusion will vary depending on whether diffusion is hindered or restricted (White, Leergaard, et al., 2013a). The acquisition parameters applied in the present study are designed to optimize the sensitivity to the different diffusion processes.

A number of quantitative metrics can be recovered from the RSI reconstruction of the diffusion data (Palmer et al., 2022b). The model estimates diffusion within different compartments, and provides metrics that are normalized into signal fractions in order to determine the relative proportion of restricted, hindered, and free water diffusion within each voxel. We focus on two metrics–the restricted normalized total signal fraction (RNT) and the hindered normalized total signal fraction (HNT).

The hindered and restricted compartments are modeled as fourth order spherical harmonic functions and the free water compartment is modelled using zeroth order spherical harmonic functions. Axial diffusivity is assumed to be constant at 1 x 10^{-3} mm^2/s for the restricted and hindered compartments. For the restricted compartment, radial diffusivity is fixed to 0 mm^2/s. For the hindered compartment, radial diffusivity is fixed to 0.9 x 10^{-3} mm^2/s. Isotropic diffusivity is fixed to 3 x 10^{-3} mm^2/s for the free water compartment. Spherical deconvolution is applied to reconstruct the fiber orientation distribution (FOD) in each voxel for the restricted compartment. The norm of the second and fourth order spherical harmonic coefficients is the restricted directional measure (RND; modeling oriented diffusion from multiple directions in a voxel), and the spherical mean of the FOD across all orientations is the restricted isotropic measure (RNI). The sum of RND and RNI is the RNT. For more details, see (Brunsing et al., 2017; Palmer et al., 2022b; White, Leergaard, et al., 2013a; White, McDonald, Farid, et al., 2013; White et al., 2014).

The two metrics extracted from RSI, RNT and HNT, can be interpreted as reflecting the relative contributions of maturational and developmental cellular processes associated with cell bodies and neurites (neural projections from the cell body such as axons and dendrites) to signal in the different compartments. These maturational and developmental processes include myelination, dendritic sprouting, changes in neurite diameter with constant neurite density, changes in cell body size with constant cell density, and changes in the concentration of mature astrocytes. Inspection of the diffusion maps of these metrics, and prior research using the same acquisition parameters in adolescents (Palmer et al., 2022b), show that RNT and HNT reliably distinguish white and grey matter and show age-related change in both tissue types (Palmer et al., 2022b). The two metrics tend to be anti-correlated. For example, increased myelination is associated with increased restricted diffusion (due to reduced permeability of axonal membranes), and decreased hindered diffusion (due to reduced volume of extracellular space). However, this is not always the case, and depends on specific tissue properties and the parcellation of signal within the different diffusion compartments in a voxel.

3 | DATA ANALYSIS

Statistical Model for FEMA and AFQ Analysis

We conducted the statistical analysis using both a fast and efficient mixed-effects algorithm (FEMA(Parekh et al., 2024) and Automated Fiber Quantification (AFQ(Yeatman et al., 2012). FEMA is a voxelwise wholebrain analysis method, and AFQ is designed for specific fiber pathways. These methods are described below. First we detail the statistical models.

The same basic model was run for three analyses: 1) the FEMA Model Main effect tested, voxelwise, the association between SRT performance and diffusion metrics; 2) the FEMA Model Interaction added the interaction term for age and SRT performance, which tests, voxelwise, where the association between SRT and diffusion metrics are moderated by age; 3) the AFQ model, which conducts the AFQ analysis to identify *where* along the specific fiber pathway performance differences are associated with diffusion metrics (by entering the interaction of SRT performance and NodeID). These models are described in Equations 1-6, and were run with RNT and HNT as outcomes, and the specified covariates. Each method is further detailed below.

$$\textbf{FEMA Model RNT Main Effect:} \quad RNT \sim \text{SRT performance} + \text{age in months} + \text{sex} + \text{hyperactivity symptoms} + \text{inattention symptoms} + \text{parent education} + \text{motion} + \text{whole brain RNT} + \varepsilon \tag{1}$$

$$\textbf{FEMA Model HNT Main Effect:} \quad HNT \sim \text{SRT performance} + \text{age in months} + \text{sex} + \text{hyperactivity symptoms} + \text{inattention symptoms} + \text{parent education} + \text{motion} + \text{whole brain HNT} + \varepsilon \tag{2}$$

$$\textbf{FEMA Model RNT Interaction:} \quad RNT \sim \text{SRT performance} * \text{age in months} + \text{sex} + \text{hyperactivity symptoms} + \text{inattention symptoms} + \text{parent education} + \text{motion} + \text{whole brain RNT} + \varepsilon \tag{3}$$

$$\textbf{FEMA Model HNT Interaction:} \quad HNT \sim \text{SRT performance} * \text{age in months} + \text{sex} + \text{hyperactivity symptoms} + \text{inattention symptoms} + \text{parent education} + \text{motion} + \text{whole brain HNT} + \varepsilon \tag{4}$$

$$\textbf{AFQ Model RNT:} \quad RNT \sim \text{SRT performance} * \text{NodeID} + \text{age in months} + \text{sex} + \text{hyperactivity symptoms} + \text{inattention symptoms} + \text{parent education} + \text{motion} + \text{whole brain RNT} + \varepsilon \tag{5}$$

$$\textbf{AFQ Model HNT:} \quad HNT \sim \text{SRT performance} * \text{NodeID} + \text{age in months} + \text{sex} + \text{hyperactivity symptoms} + \text{inattention symptoms} + \text{parent education} + \text{motion} + \text{whole brain HNT} + \varepsilon \tag{6}$$

Covariates. We included age, sex assigned at birth (sex), parental education, and ADHD symptomology (inattention and hyperactivity from the DBD (Fabiano et al., 2006a; Graziano et al., 2022)). Age, sex, and parental education were all parent reported, and the DBD measures also included teacher report. In addition, we included the whole brain diffusion metric (either RNT or HNT). Whole-brain diffusion data were output directly from the post-processing stream to control for general individual differences in diffusion properties of the brain.

Finally, we know participant movement has a substantial effect on DWI measurements, and can introduce spurious group differences in cases where none are present in the biological tissue (Yendiki et al., 2014). Therefore, incorporating movement as a nuisance regressor is recommended (Yendiki et al., 2014). To do this, we estimated movement using the root mean square (RMS) output from FSL `eddy` and implemented an overall movement cutoff for inclusion in analysis. This was arbitrarily defined as average RMS movement of more than one voxel (1.7 mm) over the course of the scan. As noted above, nineteen children (6% of the overall sample of n = 322) exceeded the movement criteria and were dropped from the sample. For participants retained in the analysis, movement was incorporated as a nuisance regressor in all analyses.

Fast and Efficient Mixed-Effects Algorithm (FEMA). We performed a whole brain, voxelwise analysis using FEMA. The algorithm is uniquely suited for large sample sizes due to its ability to efficiently perform whole-brain image-wise analyses on complex large scale imaging data (Parekh et al., 2024). It was chosen as an appropriate analysis for the current study because it is optimized for the ABCD brain atlas, and the T1-weighted MRI scans for the current study were collected according to protocol established by the ABCD study (Hagler Jr et al., 2019). The design matrix was constructed to examine the effect of SRT performance on our diffusion metrics of interest, as specified in the statistical models above. The per-voxel threshold was set at $p < 0.005$. For the interaction effect, the same basic results were obtained at $p < 0.001$, so this more stringent threshold is reported for that analysis. In order apply cluster-mass correction to correct for multiple comparisons, we repeated the analysis using FSL's `randomise` (note since this is not a multilevel model, the same results are obtained in FSL and FEMA). Both uncorrected and cluster-mass-corrected data are reported.

Automated Fiber Quantification (AFQ). Our second analysis allowed us to examine our white matter tracts of interest in-depth via Automated Fiber Quantification (AFQ). The pre-processed DWI images were analyzed by the AFQ software developed by Yeatman and colleagues (Yeatman et al., 2012), which has since been applied in a number of studies of speech fluency (Jossinger et al., 2021; Jossinger et al., 2023; Kronfeld-Duenias et al., 2016; Yablonski et al., 2019). Using the AFQ toolbox, we identified and quantified 6 bilateral white matter tracts for analysis: FAT, AF, SLFIII, ICP, MCP, and SCP. Parameters followed the AFQ protocal developed by Kruper and colleagues (Packman et al., 2022), with the addition of the bilateral frontal aslant tract as described by Kronfeld-Duenias and colleagues (Kronfeld-Duenias et al., 2016).

The implementation of the AFQ software, as described in Yeatman and colleagues (Yeatman et al., 2012), begins with the identification of regions of interest. Fiber tracts are identified using a deterministic streamline tracking algorithm and refined based on waypoint regions of interest, which define the trajectory of the fascicle. An iterative procedure cleans the bundles by removing fibers that are more than 4 standard deviations above the mean fiber length or 5 standard deviations from the core of the fiber tract. AFQ software calculates the tract profiles with a vector of one hundred values representing diffusion properties, which have been sampled at equidistant locations along the central portion of the tract.

Automatic segmentation of the FAT and SLF III was carried out using the standard AFQ regions (Yeatman et al., 2012). On visual inspection, we established new seed ROIs for the AF based on the long segment definition, as defined in (Broce et al., 2015). For the cerebellar peduncles, we used the revised protocol from Jossinger and colleagues (Jossinger et al., 2023). New ROIs defined on the Montreal Neurological Institute (MNI) template were used to identify the peduncles, together with previous ROIs established by Bruckert and colleagues (Bruckert et al., 2019). This method uses probabalistic tractography coupled with CSD modeling, which has been shown to be more successful in tracking the decussation of the cerebellar peduncles, compared to the

traditional deterministic tractography such as that used by Bruckert and colleagues (Bruckert et al., 2019; Jossinger et al., 2023). Upon visual inspection of the MCP, we modified the regions of interest to remain consistent with established definitions (Jobson et al., 2022; Nagahama et al., 2021).

After running the AFQ analysis, all data were retained for left and right FAT, SLF III, and AF. All participants were retained for left ICP, but for right ICP, 1 participant did not have a complete tract profile. For the left MCP, 3 participants had incomplete tract profiles, and 1 participant had an incomplete tract profile for the right MCP. The SCP proved to be the most difficult to track, as 39 participants had incomplete tract profiles (41 %) for the left SCP, and 32 participants had incomplete tract profiles (34 %) for the right SCP. For all incidents of missingness, we performed listwise deletion of the individual tract profile for that participant (note, these participants were retained in the whole brain analysis).

From these individual profiles, we created standardized tract profiles by calculating the mean and standard deviation of each diffusion property at each node of each tract, which we then applied to a series of generalized additive models (GAMs). GAMs have been shown to be well-suited for modeling diffusion data based on AFQ, since they account for the distribution and non-continuous nature of diffusion metrics (Muncy et al., 2022). Using this method, we identified nodes which significantly differed in diffusion properties along each white matter tract, and related these differences to SRT performance. We compared two different models to determine the best fit: one simple model calculating the main effect of SRT score on the diffusion metrics, and one that took into account the interaction of the nodes, to determine the best model fit for the current analysis. For graphing purposes, we created groups based on a median split. This allowed us to plot how diffusion metrics differed between high and low SRT scores at different node intervals. In the statistical models, SRT was entered as a continuous variable.

4 | RESULTS

4.1 | Whole Brain Analysis

We first present results for the four voxelwise FEMA models. As a brief summary, for all models only the cerebellar findings survive correction for multiple comparisons. We report uncorrected findings because several clusters were found in expected regions based on our literature review, so we focus on these clusters. In the Discussion, we consider these findings with this caveat in mind.

Figures 4 and 5 demonstrate the main effect, reporting voxels that show an association between SRT performance and either RNT or HNT. For RNT, uncorrected (Figure 4 A) whole brain voxelwise analysis revealed that speech performance on the SRT task was associated with grey and white matter cellularity in multiple regions, including bilateral IFG *pars opercularis*, right pre-SMA/SMA, FAT white matter, and bilateral cerebellum grey and white matter (the cerebellar peduncles). As Figure 4 B shows, only the cerebellar clusters survived the cluster correction. For HNT, the same regions were revealed to be associated with SRT performance. However, the cerebellar clusters were smaller, and in fact no clusters survived statistical correction (Figure 4 A and B).

Figures 6 and 7 show the results for the interaction effect. Note these are reported for the more strict $p < .001$ threshold, as the cluster-corrected findings were the same for the $p < .005$ level. Age moderated the association between SRT and both RNT and HNT in left frontal aslant tract, bilateral caudate, right globus pallidus, and large parts of bilateral cerebellum. For RNT, there was an additional cluster in left *pars opercularis*. In both RNT and HNT analyses, only the cerebellar clusters survived multiple comparison correction (B in both Figures). Figure 8 shows the nature of this interaction for the clusters revealed in cerebellum.

4.2 | AFQ Analysis

To further probe the relationship between SRT performance and diffusion metrics along each white matter tract, we examined the tract profiles of white matter pathways identified in our literature review as potentially important for speech. Thus, AFQ analysis was conducted on the FAT, SLFIII, AF, ICP, MCP, and SCP.

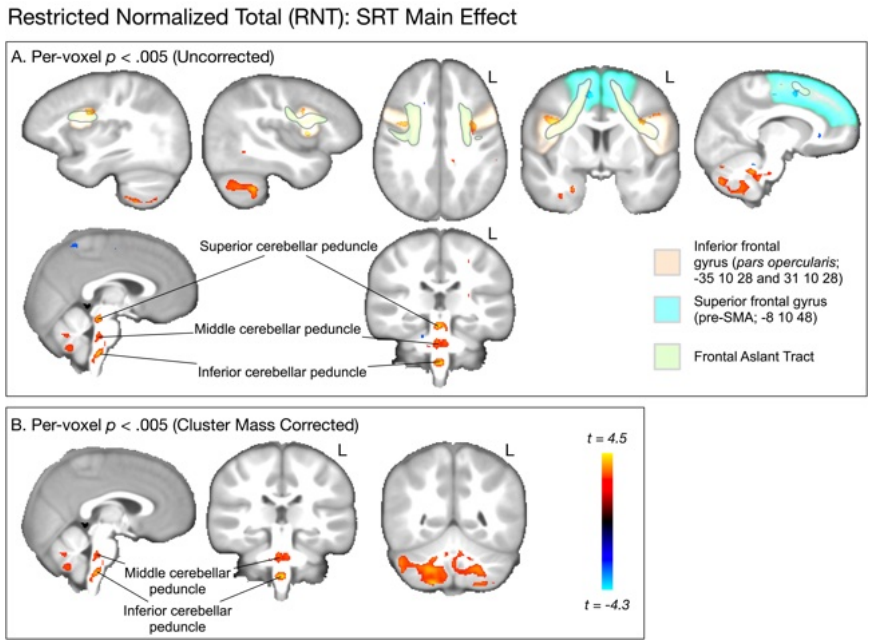

FIGURE 4 Whole brain, voxelwise analysis of the main effect association between SRT performance and RNT (Model Equation 1). A. Uncorrected ($p < .005$) clusters are highlighted for regions and pathways reviewed in the introduction. Areas in red spectrum indicate a positive association between SRT performance and grey and white matter cellular properties, as measured by RNT. Blue indicates a negative association between SRT performance and RNT. B. Cluster mass corrected ($p < .005$) results show only clusters in cerebellar grey and white matter.

Our primary aim for this analysis was to examine the association between SRT performance and diffusion properties. Since there are 100 nodes along the tract profile, rather than conducting separate tests for each node, we examined each tract in a series of GAM models. We were mainly interested in whether SRT performance was moderated by placement (NodeID) along the tract profile. That is, we sought to examine whether performance differences were evident at certain points along the tract, but not others. Thus, for each tract we modeled a main effect of SRT predicting diffusion, and a second model in which the interaction of SRT and NodeID was tested. Using ANOVA, we tested whether including the interaction explained significantly more variance (deviance) than the model with only the main effect of SRT. Table 1 demonstrates that for all tracts, including the interaction term explained significantly more variance (all F tests comparing the two models were significant at $p < .001$). This means that associations between SRT and diffusion properties differed in magnitude depending on placement along the tract profile.

With these interaction effects established, we conducted differences tests (essentially dependent samples t-tests) at each node, assessing high vs. low performing participants (defined by the median split). Because this amounts to 100 tests for each tract, we corrected for multiple comparisons using the false discovery rate (FDR; (Benjamini & Hochberg, 1995) procedure. These tract profiles are shown in Figures 9 and 11 (for cortical association pathways) and Figure 10 and 12 (for cerebellar pathways). In the figures, blue marks Node IDs that survived the FDR correction. In general, the results were similar for RNT and HNT, just in opposite directions.

As the Figures show, for FAT significant nodes were identified along the tract and highlighted in blue. No significant nodes were identified for the right FAT.

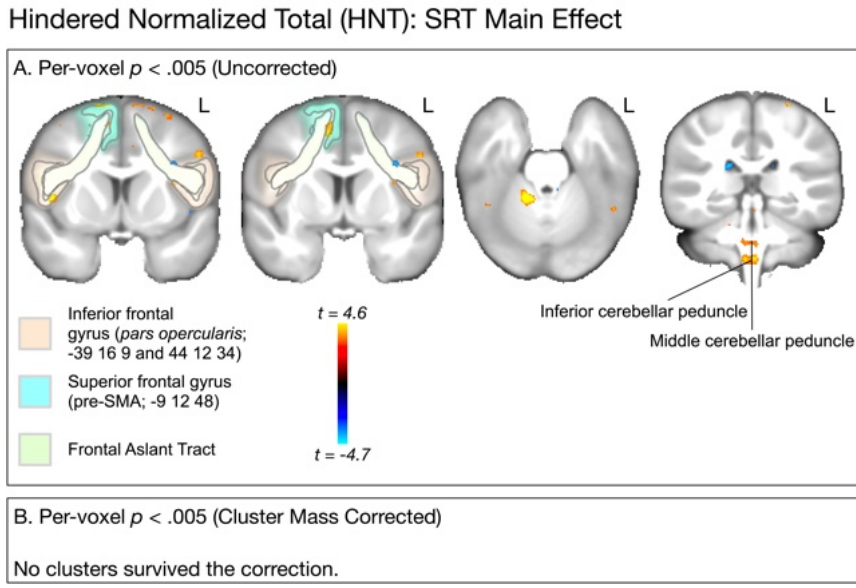

FIGURE 5 Whole brain, voxelwise analysis of the main effect association between SRT performance and HNT (Model Equation 2). A. Uncorrected ($p < .005$) clusters are highlighted for regions and pathways reviewed in the introduction. Areas in red spectrum indicate a positive association between SRT performance and grey and white matter cellular properties, as measured by RNT. Blue indicates a negative association between SRT performance and RNT. B. No voxels survived cluster mass correction ($p < .005$).

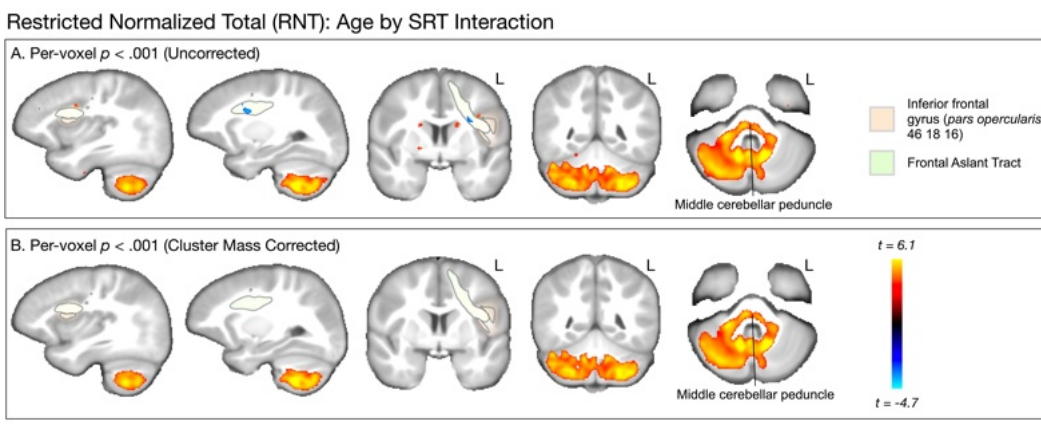

FIGURE 6 Whole brain, voxelwise analysis of the interaction effect showing how age moderates the association between SRT performance and RNT (Model Equation 3). A. Uncorrected ($p < .001$) clusters are highlighted for regions and pathways reviewed in the introduction. Areas in red spectrum indicate a positive interaction slope, and blue indicates a negative interaction slope. B. Cluster mass corrected ($p < .001$) results show only clusters in cerebellar grey and white matter.

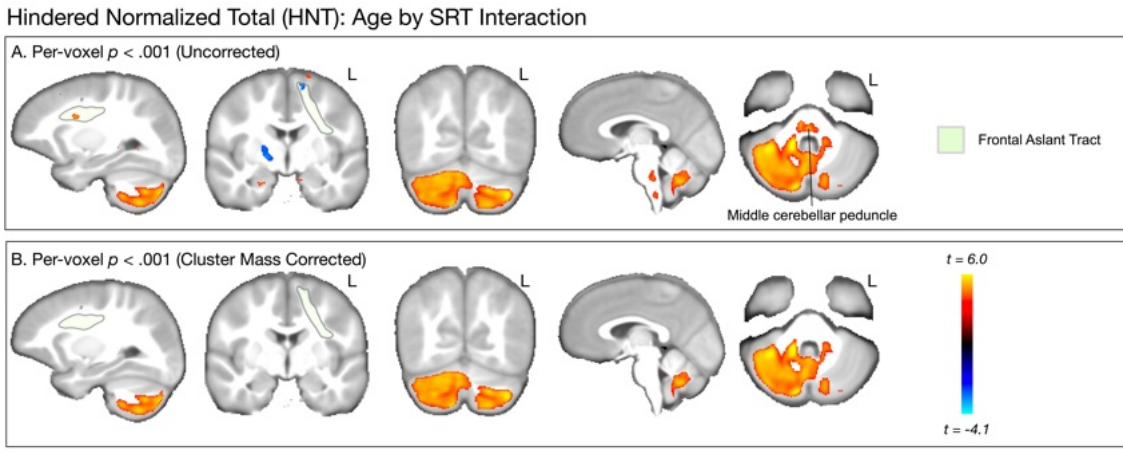

FIGURE 7 Whole brain, voxelwise analysis of the interaction effect showing how age moderates the association between SRT performance and HNT (Model Equation 4). A. Uncorrected ($p < .001$) clusters are highlighted for regions and pathways reviewed in the introduction. Areas in red spectrum indicate a positive interaction slope, and blue indicates a negative interaction slope. B. Cluster mass corrected ($p < .001$) results show only clusters in cerebellar grey and white matter.

Although no significant clusters were identified in AF and SLF III in the whole brain analysis, fiber tract segmentation revealed significant RNT differences between Above and Below Median SRT performance groups at considerable intervals along the tract profiles for SLF III, especially on the right hemisphere. In fact, no differences were found in left SLF III for the HNT metric. There were also significant differences in SRT performance for the left and right AF tract profiles, but these were not extensive, and were at isolated points along the tract.

We also examined significant differences in RNT between SRT performance groups for the cerebellar peduncles. The bilateral SCP and ICP both contained large intervals with significant differences at those nodes. For MCP, differences were only found on the left (for RNT), but bilaterally for HNT.

5 | DISCUSSION

Updated models of speech implicate a network of grey matter regions and the white matter pathways that connect them in speech production and speech perception. Despite progress in identifying these regions and pathways, there are many questions that remain about how this speech network develops in early childhood. We examined this development in 4-7-year-olds (some diagnosed with ADHD) who varied considerably in speech ability as measured by a speech task, the SRT. Our results revealed several key findings: 1) performance on the SRT is associated with differences in grey matter cellularity in regions identified as critical for speech perception and production; 2) performance on the SRT further predicts differences in diffusion metrics along white matter tracts related to speech perception and production; 3) the association between speech task performance and grey and white matter cellularity changes as a function of age.

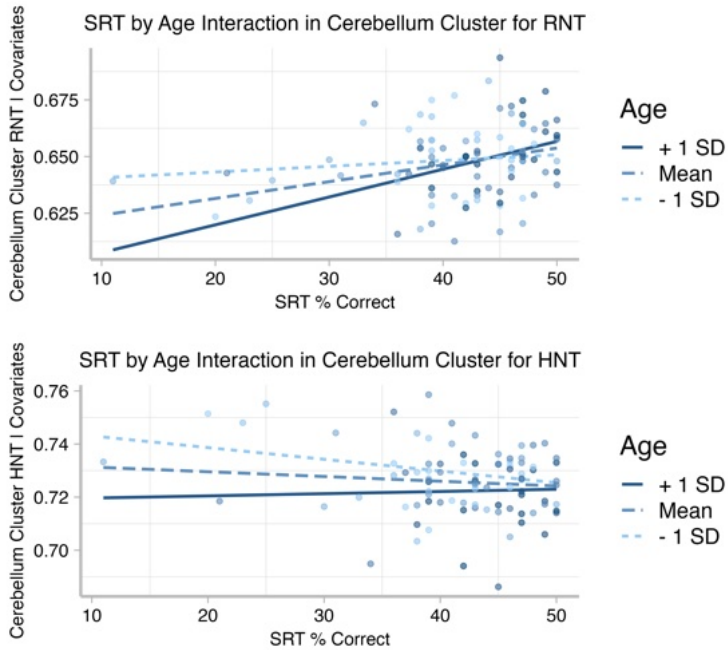

FIGURE 8 Residualized scatterplots show that age moderates the association between (top) SRT performance and Restricted Diffusion; and (bottom) SRT performance and Hindered Diffusion in the cerebellum. Data are recovered from the cluster-corrected voxels for the whole-brain interaction analysis, for each participant.

5.1 | Performance on the SRT is associated with cellularity differences in frontal brain regions and pathways associated with speech

In the analysis of the whole-brain data, we found that 1) higher RNT in bilateral *pars opercularis* was associated with better performance on the SRT; 2) reduced RNT and increased HNT in right pre-SMA/SMA was associated with better performance on the SRT. Notably, neither of these findings survived multiple comparison correction, although these were regions predicted by our literature review. Based on this, we feel it is appropriate to discuss them with appropriate caveats in mind. We will examine the findings in *pars opercularis* first before discussing the pre-SMA/SMA finding.

Left *pars opercularis* is a prominent node in most models of speech neurobiology. For example, in GODIVA (Guenther, 2016), parts of this region may contain cell populations representing syllable motor programs independent of semantic content (Ghosh et al., 2008). In Hickok's model (Hickok et al., 2023), the *pars opercularis* is proposed to be involved in the sequencing of syllables. Our findings in left *pars opercularis* are consistent with these models. However, our findings for RNT are also bilateral. One reason for the similar association found in right *pars opercularis* may be due to the age of the participants. Indeed, although the brain may be primed for left lateralization of language function from birth, left lateralization also appears to show age related differences, increasing over the course of development (Olulade et al., 2020). In an earlier study, Holland and colleagues (S. K. Holland et al., 2001) showed that left lateralization in inferior frontal cortex increased with age from 7-18-years during a verb generation task. More recently, Olulade and colleagues (Olulade et al., 2020) showed that strong activation in right hemisphere homologues during fMRI language paradigms is evident for younger children (e.g., 4-8-years), but declines through adolescence into adulthood. This was particularly apparent for right inferior frontal cortex. They suggested that the right hemisphere contribution to language in early childhood is substantial, which is consistent with the findings we report. In addition, age moderated the association between SRT performance an RNT in left *pars opercularis*, with the association becoming stronger in older children. This is consistent with

TABLE 1 Model Fit Indices and Comparisons for Each Tract Profile

Tract	*F* (*p*-value)	Main Effect AIC	% Deviance Explained (ME)	Interaction AIC	% Deviance Explained (Int)
Left FAT	9.1 ***	-33293.9	84.4	-33815.3	85.4
Right FAT	8.8 ***	-34275.3	85.9	-34756.8	86.7
Left AF	6.8 ***	-17568.4	43.7	-17878.1	46.4
Right AF	9.2 ***	-16672.4	31.2	-17138.4	35.2
Left SLF III	8.7 ***	-31870.7	70.8	-32314.8	72.5
Right SLF III	7.9 ***	-30573.8	68.7	-30937.1	70.2
Left SCP	9.7 ***	-3850.8	13.7	-4296.7	21.2
Right SCP	8.91 ***	-6406.8	14.0	-6827.3	20.8
Left MCP	7.07 ***	-7257.1	25.7	-7539.2	28.3
Right MCP	7.37 ***	-7516.1	28.8	-7821.1	31.5
Left ICP	12.4 ***	-27445.7	53.2	-28132.1	57.0
Right ICP	16.8 ***	-14909.4	24.6	-15979.6	33.3

Note. *** = $p < .001$; AIC = Akaike Information Criterion; ME = Main Effect, Int = Interaction Effect. FAT = Frontal Aslant Tract. AF = Arcuate Fasciculus; SLF III = Superior Longitudinal Fasciculus III; SCP, MCP, ICP = Superior, Middle, and Inferior Cerebellar Peduncles.

the notion that left laterality emerges over development.

Interpreting the meaning of the association between the restricted diffusion signal and performance is speculative, but we can make some initial guesses based on histologic findings investigating the RSI model. Palmer and colleagues (Palmer et al., 2022a) investigated age-related changes in restricted diffusion in adolescents, and suggested that increases in restricted diffusion in grey matter regions with age could be driven by increases in myelination, neurite density (axons and dendrites), dendritic sprouting, or increases in the size of cell bodies (either neuronal or glial). White and colleagues (White, Leergaard, et al., 2013b; White, McDonald, Farid, et al., 2013; White et al., 2014) original studies developing the RSI model suggest sensitivity of the restricted component to these tissue properties. Thus, we can speculatively suggest that the associations we find between SRT performance and RNT from the RSI model are reflective of these microstructural properties, but we are unable to provide any further specificity without histologic data.

In the FAT white matter, we can speculate these associations have more to do with myelination of the pathway, which reduces the volume of extracellular space and also reduces the permeability of axonal membranes. This would lead to increased signal in the restricted compartment. The AFQ analysis of the FAT showed that this effect was predominantly unilateral. In fact, no performance differences in the right FAT were statistically significant after FDR correction. Thus, unlike the finding in *pars opercularis* grey matter, the finding in FAT was prominently left lateralized. Moderating effects of age were also left lateralized. It is possible that for FAT white matter, connecting inferior frontal gyrus and pre-SMA/SMA cortical regions, the left FAT is more critical for speech than the right FAT (Dick et al., 2019). This is suggested by investigations in adults, which have shown that left FAT integrity is associated with stuttering (Kemerdere et al., 2016; Kronfeld-Duenias et al., 2016; Misaghi et al., 2018), speech arrest during tumor resection and intraopertive electrostimulation (Fujii et al., 2015; Vassal et al., 2014), post-stroke aphasia (Basilakos et al., 2014), and apraxia of speech (Zhong et al., 2022b). In this latter study, damage to the white matter and not the grey matter was the best predictor of speech impairment, suggesting that disconnection of the connectivity is a stronger factor for predicting motor speech deficits. Our findings are consistent with this possibility.

We also found a small cluster in right pre-SMA/SMA showing an association between SRT performance and reduced RNT/increased

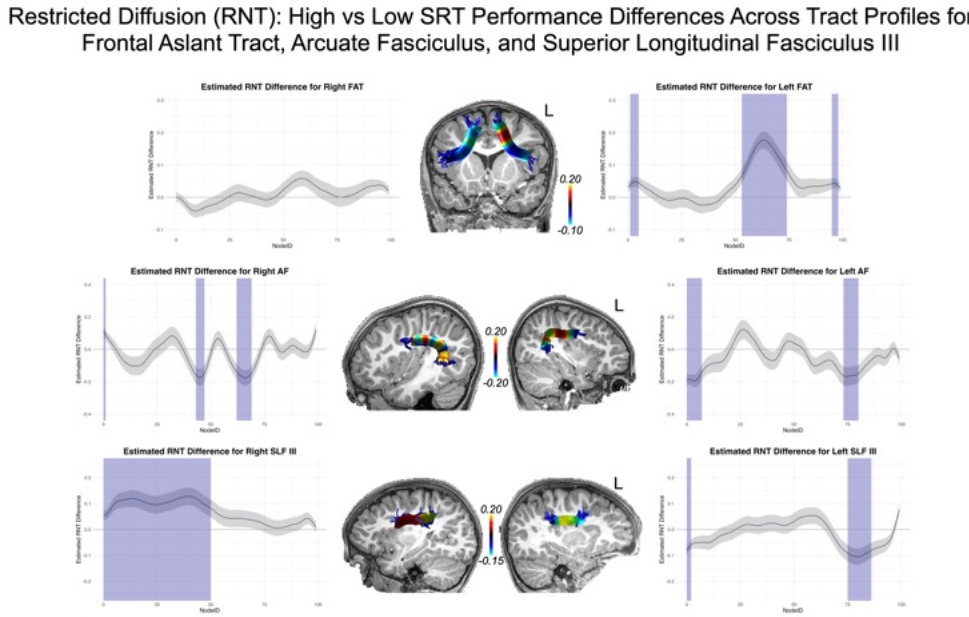

FIGURE 9 High vs Low Syllable Repetition Task performance differences across tract profiles for Frontal Aslant Tract (FAT), Arcuate Fasciculus (AF), and Superior Longitudinal Fasciculus III (SLF III), for the Restricted Diffusion (RNT) metric. The y-axis reports the difference score for high versus low performers determined by median split. The x-axis reports the Node Index for the 100 nodes along the tract profile. Blue indicates the difference was statistically significant after false discovery rate (FDR) correction. The difference scores from the statistical analysis are mapped to representative tracts overlaid on T1 images for each tract.

HNT. Again, this cluster was small and did not survive cluster correction. However, the involvement of this region is consistent with what we know about involvement of bilateral pre-SMA/SMA in speech production (Alario et al., 2006; Bohland & Guenther, 2006; Tremblay & Gracco, 2009, 2010). For example, stimulation of pre-SMA/SMA during awake surgery causes speech arrest (Lu et al., 2021), and Bohland and Guenther (Bohland & Guenther, 2006) showed that even for production of simple syllable sequences, the basic speech production network includes bilateral pre-SMA and SMA. It is more difficult to understand the direction of the effect–less restricted diffusion (and more hindered diffusion) in this region was associated with better performance, which is the opposite direction of the other effects we found. Changes in diffusion properties may reflect a number of different microstructural changes. For example, increased dendritic pruning, which might lead to better processing efficiency of neural assemblies in pre-SMA/SMA, would lead to reduced restricted diffusion signal, and increased hindered diffusion signal. It is possible that this association reflects such a process, but this speculation would need histological validation.

5.2 | Performance on the SRT is associated with cellularity differences in cerebellar white and grey matter

The whole brain analysis revealed that 1) higher RNT and HNT in bilateral Crus I and II was associated with better SRT performance; and 2) higher RNT and HNT was associated with cerebellar white matter pathways: the SCP (for RNT only), MCP, and ICP. While for RNT, findings from cerebellar grey matter and MCP/ICP survived cluster correction, the SCP clusters did not (no clusters survived for HNT). Thus, associations with SCP should be interpreted with this caveat in mind.

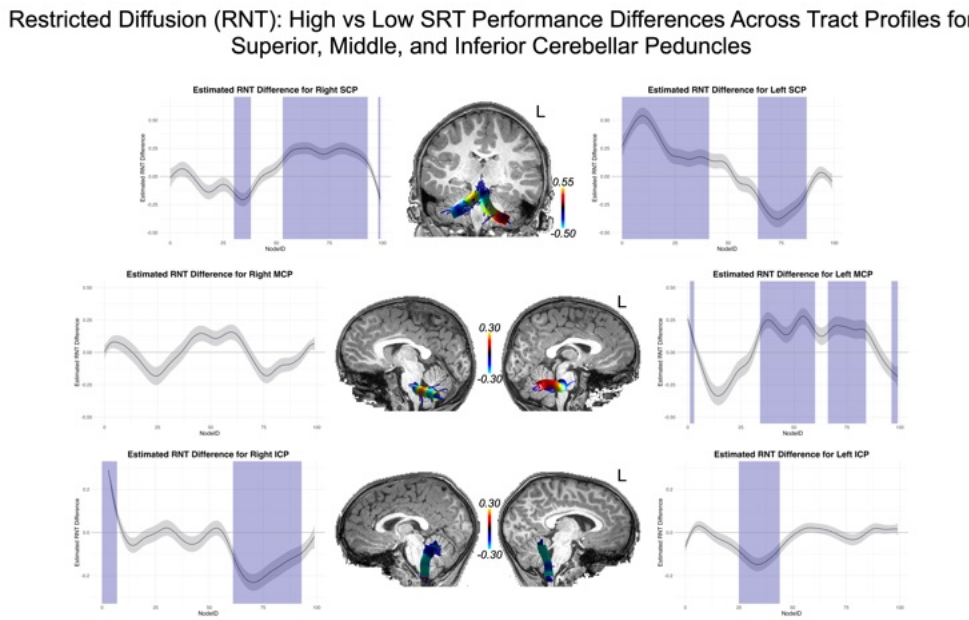

FIGURE 10 High vs Low Syllable Repetition Task performance differences across tract profiles for Superior (SCP), Middle (MCP), and Inferior (ICP) Cerebellar Peduncles, for the Restricted Diffusion (HNT) metric. The y-axis reports the difference score for high versus low performers determined by median split. The x-axis reports the Node Index for the 100 nodes along the tract profile. Blue indicates the difference was statistically significant after false discovery rate (FDR) correction. The difference scores from the statistical analysis are mapped to representative tracts overlaid on T1 images for each tract.

The role of the cerebellum in speech motor control has long been attributed to the organization and coordination of motor commands necessary for speech production, but is particularly important for rapid speech (Ackermann, 2008; Guenther, 2016) or for more complex syllable sequences (Bohland & Guenther, 2006). The developmental importance of finely timed speech has been demonstrated in studies of children with early speech deficits, which found that poorer speech outcomes were associated with right cerebellar tumors (A. Morgan et al., 2011). This is consistent with adult cerebellar lesion studies (Urban et al., 2003), and the established connectivity of inferior frontal regions with the contralateral right cerebellum (A. Morgan et al., 2011). Results from the present study indicated bilateral findings in the grey matter of the cerebellum, especially in the Crus I and Crus II cerebellar lobules. However, fMRI activation during speech and foci collected from meta-analyses of word and sentence reading have highlighted bilateral associations between speech and cerebellar grey matter (Brown et al., 2005; Guenther, 2016; Turkeltaub et al., 2002). Further, bilateral activation of Crus I and Crus II during speech production tasks has been reported (Bohland & Guenther, 2006; Correia et al., 2020; Geva et al., 2021; Ghosh et al., 2008; Peeva et al., 2010; Shuster & Lemieux, 2005). Thus, our findings are in line with previous literature that suggests motor control of speech is not limited to the right cerebellum.

The connectivity of the cerebellum with cortical and subcortical structures in the cerebral cortex is established through the cerebellar peduncles, bilateral white matter tracts that have been shown to play a role in aspects of speech fluency and motor speech production (Guenther, 2016; Johnson et al., 2022; Jossinger et al., 2023). Jossinger and colleagues investigated the role of the cerebellar peduncles in different components of speech processing, and found that verbal fluency was associated with the right SCP, whereas speaking rate was associated with the right MCP (Jossinger et al., 2023). A similar pattern is observed in children who stutter, as early developmental differences have been demonstrated between children who stutter and their age-matched peers in the right ICP (Johnson et al., 2022). However, the association between the cerebellar peduncles and motor

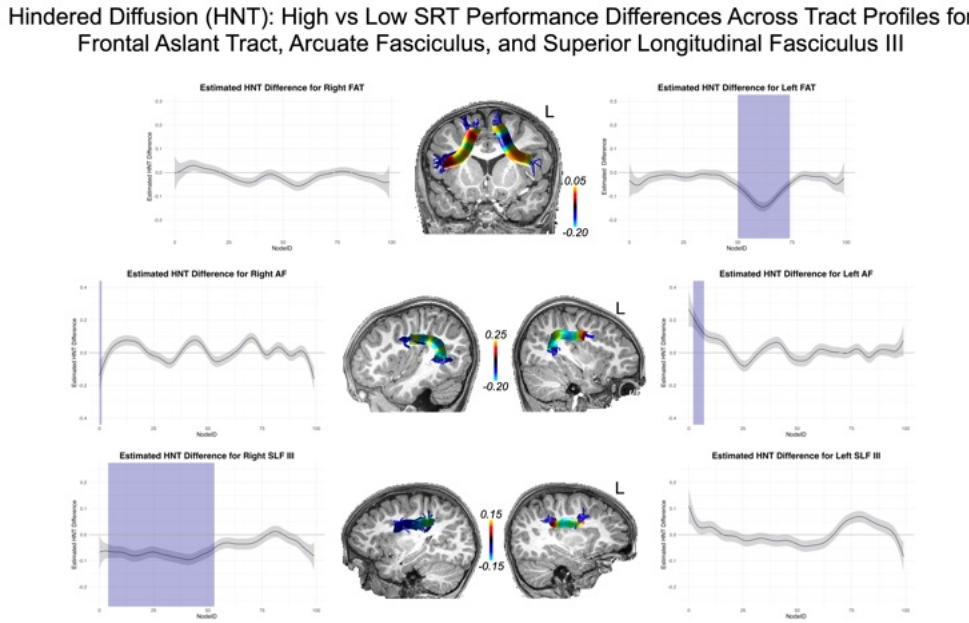

FIGURE 11 High vs Low Syllable Repetition Task performance differences across tract profiles for Frontal Aslant Tract (FAT), Arcuate Fasciculus (AF), and Superior Longitudinal Fasciculus III (SLF III), for the Hindered Diffusion (HNT) metric. The y-axis reports the difference score for high versus low performers determined by median split. The x-axis reports the Node Index for the 100 nodes along the tract profile. Blue indicates the difference was statistically significant after false discovery rate (FDR) correction. The difference scores from the statistical analysis are mapped to representative tracts overlaid on T1 images for each tract.

speech production is not restricted to the right cerebellar peduncles. In adults who stutter, speech rate has been associated with white matter cellular properties in the left ICP (Jossinger et al., 2021). Further, reduced white matter integrity has been observed bilaterally for all three cerebellar peduncles in adolescents and adults who stutter (Connally et al., 2014), dispelling the notion that motor speech production is necessarily right lateralized. Our bilateral findings in the SCP, MCP, and ICP support the idea that key aspects of speech production may be organized bilaterally within the white matter pathways that connect the cerebellum to the cerebral cortex. The findings in the SCP from the whole brain analysis did not survive cluster correction, but our analysis of the SCP tract profiles revealed several significant nodes, which suggests that there may be some relationship between white matter cellular properties and speech performance that requires additional study to tease apart. While both the left and right ICP displayed significant nodes, only the left MCP demonstrated a difference in SRT performance across the nodes. It is possible that we observed these differences because the cerebellar peduncles play distinct roles in motor speech processing, as noted by Jossinger and colleagues (Jossinger et al., 2023), but understanding this relationship requires further analysis of different speech properties.

The findings from the present study demonstrate that greater differences in performance on a speech task involving speech perception and production is associated with higher RNT and HNT in grey matter of the cerebellum, and higher RNT and lower HNT in white matter of the cerebellar peduncles (based on the tract profile analysis). Based on our knowledge of how RSI modulates developmental and maturational processes, we can speculate on the nature of the association, but we are unable to make definitive claims about the relationship between the restricted diffusion signal and speech performance without using more direct measurements. Developmental processes such as dendritic sprouting, myelination, and increasing neurite diameter result in a decrease in extracellular space, which in turn causes the signal to increase within the cellular compartment (Palmer et

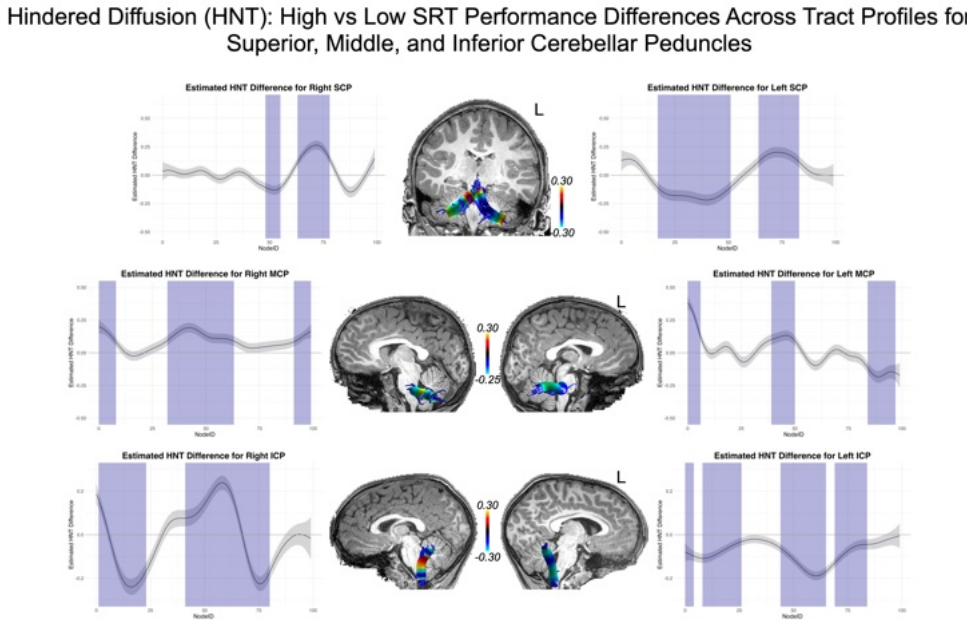

FIGURE 12 High vs Low Syllable Repetition Task performance differences across tract profiles for Superior (SCP), Middle (MCP), and Inferior (ICP) Cerebellar Peduncles, for the Hindered Diffusion (HNT) metric. The y-axis reports the difference score for high versus low performers determined by median split. The x-axis reports the Node Index for the 100 nodes along the tract profile. Blue indicates the difference was statistically significant after false discovery rate (FDR) correction. The difference scores from the statistical analysis are mapped to representative tracts overlaid on T1 images for each tract.

al., 2022b). In particular, higher myelination is associated with greater speed of conductance for information traveling between neurons (Jossinger et al., 2021; Palmer et al., 2022a; Zhong et al., 2022a). We may tentatively conclude that an increase in RNT and decrease in HNT, possibly driven by developmental processes such as myelination, could lead to faster conduction of information and thus better performance on a speech task. This would be in line with the results from our whole brain analysis, which suggested that higher restricted diffusion signal was positively associated with speech performance, and that age moderated the strength of this association, which increased with age. While these conclusions are speculative, understanding the relationship between microstructural properties of grey and white matter and speech performance allows us to establish a relationship that may be further investigated in the future.

5.3 | Tract profile analysis reveals more detailed relationship between SRT performance and dorsal stream fiber pathways

Although the whole brain analysis did not demonstrate any significant associations between SRT performance and AF and SLF III, the AFQ analysis revealed significant differences in RNT between Above Median and Below Median SRT groups, although the differences were largely negligible for AF. The AF and SLF III both have established connectivity of regions putatively important for motor speech function, such as the IFG and STS/STG (Bernal & Ardila, 2009; Duffau et al., 2003; Hickok & Poeppel, 2004, 2007). We may speculate that the observed differences between Above Median and Below Median SRT performance groups provide converging evidence for the role of the AF and SLF III in motor speech function. It is important to interpret these results with caution, since we have found GAMs to be extremely sensitive to small differences, and we did not observe any associations

between RNT and speech performance in the AF or SLF III in our whole brain analysis. However, these results are still critical to our understanding of the neural speech network. While traditional fiber tracking that averages diffusion metrics across the entire fiber bundle are common, they may fail to recognize relationships that may be revealed by tracking diffusion metrics at different points along the tract. Diffusion metrics have been shown to vary along the tract trajectory (Yeatman et al., 2011), so by creating tract profiles that establish node intervals of significance along each tract, we can parse out a relationship that may not be visible with traditional fiber bundle averaging. Thus, investigating white matter tracts with methods such as AFQ is a critical step to providing a more complete picture of the relationship between white matter microstructural properties and diffusion metrics.

5.4 | Limitations

One limitation of the current study regards the sample makeup, which included both children who are typically developing and children with ADHD, and contained a higher percentage of boys than girls. Children who are atypically developing, such as those with ADHD, are at high risk for developing comorbid psychiatric and speech disorders (Booster et al., 2012), and a mixed sample over-represented by boys may not be generalizable to a broader population. However, few studies focusing on the development of neural speech networks in early childhood exist, and the findings from this study provide critical background for understanding the implementation of speech perception and production in the brain at early stages of speech development. We did not find performance differences on the SRT, and we further controlled for ADHD symptomology. This suggests that treating the ADHD and TD children as a representative sample for performance on this task is justified.

A second limitation concerns the speech task implemented in the current research, the SRT. For this study, we focused on a single speech task that measured the repetition of multisyllabic utterances. Although the SRT measures expressive speech production and auditory-perceptual speech processing (Shriberg et al., 2009), it is not sensitive to the different phases of speech that may occur during repetition. For example, the SRT is unable to distinguish between prearticulatory encoding, and the actual transformation of phonological planning into motor execution of speech. The SRT is also a speech task that measures the repetition of single, multisyllabic nonwords, and thus cannot provide insight into how connected speech may play a role in speech processing. Despite these limitations, the SRT is a child-friendly phonemic task that has been validated as an assessment of motor planning difficulties (Rvachew & Matthews, 2017), and may be considered as part of a battery of speech and language tasks in the future to provide a more complete picture of speech development.

Finally, we must carefully consider what our diffusion metrics of interest actually measure. Although we can provide speculation for what cellular processes are modulated by restricted and hindered diffusion, we cannot definitively identify the developmental and maturational processes underlying differences in diffusion metrics. The issue of specificity is a problem for diffusion measures more broadly, not just RSI. In fact, a major strength of RSI beyond traditional diffusion measures, such as diffusion tensor imaging (DTI), is that we are able to observe differences in cellularity in both grey and white matter. While RSI has its constraints, much like other DWI reconstruction methods, it provides a more complete picture of neural development across grey matter regions of interest and white matter pathways.

6 | CONCLUSION

Characterizing the structural development of the neural speech network in early childhood is important for understanding speech acquisition. In this investigation, we found that 1) performance on the SRT is associated with differences in grey matter cellularity in regions identified as critical for speech perception and production, including inferior frontal gyrus and pre-SMA/SMA and especially in cerebellum; 2) performance on the SRT further predicts differences in diffusion metrics along white matter tracts related to speech perception and production, especially left FAT and the cerebellar peduncles; 3) the association between speech task performance and grey and white matter cellularity changes as a function of age in these regions and pathways. The findings suggest that individual differences in speech performance are reflected in structural gray and white matter differences

as measured by restricted and hindered diffusion properties, and offer important insights into how the neural speech network develops in children during early childhood.

6.1 | Conflict of Interest

Authors report no conflict of interest.

6.2 | Acknowledgments

We thank the parents and children who participated in the AHEAD study from which these data were analyzed.

References

Ackermann, H. (2008). Cerebellar contributions to speech production and speech perception: Psycholinguistic and neurobiological perspectives. *Trends in neurosciences*, *31*(6), 265–272.

Alario, F.-X., Chainay, H., Lehericy, S., & Cohen, L. (2006). The role of the supplementary motor area (sma) in word production. *Brain research*, *1076*(1), 129–143.

Andersson, J. L., Graham, M. S., Drobnjak, I., Zhang, H., Filippini, N., & Bastiani, M. (2017). Towards a comprehensive framework for movement and distortion correction of diffusion mr images: Within volume movement. *Neuroimage*, *152*, 450–466.

Andersson, J. L., Graham, M. S., Zsoldos, E., & Sotiropoulos, S. N. (2016). Incorporating outlier detection and replacement into a non-parametric framework for movement and distortion correction of diffusion mr images. *Neuroimage*, *141*, 556–572.

Andersson, J. L., Skare, S., & Ashburner, J. (2003). How to correct susceptibility distortions in spin-echo echo-planar images: Application to diffusion tensor imaging. *Neuroimage*, *20*(2), 870–888.

Bammer, R., Markl, M., Barnett, A., Acar, B., Alley, M., Pelc, N., Glover, G., & Moseley, M. (2003). Analysis and generalized correction of the effect of spatial gradient field distortions in diffusion-weighted imaging. *Magnetic Resonance in Medicine: An Official Journal of the International Society for Magnetic Resonance in Medicine*, *50*(3), 560–569.

Barbeau, E. B., Descoteaux, M., & Petrides, M. (2020). Dissociating the white matter tracts connecting the temporo-parietal cortical region with frontal cortex using diffusion tractography. *Scientific reports*, *10*(1), 8186.

Barnett, A. S., Hutchinson, E., Irfanoglu, M. O., & Pierpaoli, C. (n.d.). Higher order correction of eddy current distortion in diffusion weighted echo planar images. *Join Annual Meeting ISMRM-ESMRMB, Milan, Italy*, 5119.

Barnett, A. S., Irfanoglu, M. O., Landman, B., Rogers, B., & Pierpaoli, C. (2021). Mapping gradient nonlinearity and miscalibration using diffusion-weighted mr images of a uniform isotropic phantom. *Magnetic resonance in medicine*, *86*(6), 3259–3273.

Basilakos, A., Fillmore, P. T., Rorden, C., Guo, D., Bonilha, L., & Fridriksson, J. (2014). Regional white matter damage predicts speech fluency in chronic post-stroke aphasia. *Frontiers in human neuroscience*, *8*, 845.

Benjamini, Y., & Hochberg, Y. (1995). Controlling the false discovery rate: A practical and powerful approach to multiple testing. *Journal of the royal statistical society. Series B (Methodological)*, 289–300.

Bernal, B., & Altman, N. (2009). Neural networks of motor and cognitive inhibition are dissociated between brain hemispheres: An fmri study. *International Journal of Neuroscience*, *119*(10), 1848–1880.

Bernal, B., & Ardila, A. (2009). The role of the arcuate fasciculus in conduction aphasia. *Brain*, *132*(9), 2309–2316.

Bernard, F., Zemmoura, I., Ter Minassian, A., Lemée, J.-M., & Menei, P. (2019). Anatomical variability of the arcuate fasciculus: A systematical review. *Surgical and radiologic anatomy*, *41*, 889–900.

Bihan, D. L. (1995). Molecular diffusion, tissue microdynamics and microstructure. *NMR in Biomedicine*, *8*(7), 375–386.

Bohland, J. W., & Guenther, F. H. (2006). An fmri investigation of syllable sequence production. *Neuroimage*, *32*(2), 821–841.

Booster, G. D., DuPaul, G. J., Eiraldi, R., & Power, T. J. (2012). Functional impairments in children with adhd: Unique effects of age and comorbid status. *Journal of Attention Disorders*, *16*(3), 179–189.

Broce, I., Bernal, B., Altman, N., Tremblay, P., & Dick, A. S. (2015). Fiber tracking of the frontal aslant tract and subcomponents of the arcuate fasciculus in 5–8-year-olds: Relation to speech and language function. *Brain and language*, *149*, 66–76.

Brown, S., Ingham, R. J., Ingham, J. C., Laird, A. R., & Fox, P. T. (2005). Stuttered and fluent speech production: An ale meta-analysis of functional neuroimaging studies. *Human brain mapping*, *25*(1), 105–117.

Bruckert, L., Shpanskaya, K., McKenna, E. S., Borchers, L. R., Yablonski, M., Blecher, T., Ben-Shachar, M., Travis, K. E., Feldman, H. M., & Yeom, K. W. (2019). Age-dependent white matter characteristics of the cerebellar peduncles from infancy through adolescence. *The Cerebellum*, *18*, 372–387.

Brunsing, R. L., Schenker-Ahmed, N. M., White, N. S., Parsons, J. K., Kane, C., Kuperman, J., Bartsch, H., Kader, A. K., Rakow-Penner, R., & Seibert, T. M. (2017). Restriction spectrum imaging: An evolving imaging biomarker in prostate mri. *Journal of Magnetic Resonance Imaging*, *45*(2), 323–336.

Buchsbaum, B. R., Hickok, G., & Humphries, C. (2001). Role of left posterior superior temporal gyrus in phonological processing for speech perception and production. *Cognitive science*, *25*(5), 663–678.

Catani, M., Mesulam, M. M., Jakobsen, E., Malik, F., Martersteck, A., Wieneke, C., Thompson, C. K., Thiebaut de Schotten, M., Dell'Acqua, F., & Weintraub, S. (2013). A novel frontal pathway underlies verbal fluency in primary progressive aphasia. *Brain*, *136*(8), 2619–2628.

Chang, H., & Fitzpatrick, J. M. (1992). A technique for accurate magnetic resonance imaging in the presence of field inhomogeneities. *IEEE transactions on medical imaging*, *11*(3), 319–329.

Chang, S.-E., Zhu, D. C., Choo, A. L., & Angstadt, M. (2015). White matter neuroanatomical differences in young children who stutter. *Brain*, *138*(3), 694–711.

Cohen, J. (1960). A coefficient of agreement for nominal scales. *Educational and psychological measurement*, *20*(1), 37–46.

Connally, E. L., Ward, D., Howell, P., & Watkins, K. E. (2014). Disrupted white matter in language and motor tracts in developmental stuttering. *Brain and language*, *131*, 25–35.

Correia, J. M., Caballero-Gaudes, C., Guediche, S., & Carreiras, M. (2020). Phonatory and articulatory representations of speech production in cortical and subcortical fmri responses. *Scientific Reports*, *10*(1), 4529.

Dick, A. S., Garic, D., Graziano, P., & Tremblay, P. (2019). The frontal aslant tract (fat) and its role in speech, language and executive function. *Cortex*, *111*, 148–163.

Duffau, H., Gatignol, P., Denvil, D., Lopes, M., & Capelle, L. (2003). The articulatory loop: Study of the subcortical connectivity by electrostimulation. *Neuroreport*, *14*(15), 2005–2008.

Fabiano, G. A., Pelham, W. E., Jr, Waschbusch, D. A., Gnagy, E. M., Lahey, B. B., Chronis, A. M., Onyango, A. N., Kipp, H., Lopez-Williams, A., & Burrows-MacLean, L. (2006a). A practical measure of impairment: Psychometric properties of the impairment rating scale in samples of children with attention deficit hyperactivity disorder and two school-based samples. *Journal of Clinical Child and Adolescent Psychology*, *35*(3), 369–385.

Fabiano, G. A., Pelham, W. E., Jr, Waschbusch, D. A., Gnagy, E. M., Lahey, B. B., Chronis, A. M., Onyango, A. N., Kipp, H., Lopez-Williams, A., & Burrows-MacLean, L. (2006b). A practical measure of impairment: Psychometric properties of the impairment rating scale in samples of children with attention deficit hyperactivity disorder and two school-based samples. *Journal of Clinical Child and Adolescent Psychology*, *35*(3), 369–385.

Frings, M., Dimitrova, A., Schorn, C. F., Elles, H.-G., Hein-Kropp, C., Gizewski, E. R., Diener, H. C., & Timmann, D. (2006). Cerebellar involvement in verb generation: An fmri study. *Neuroscience letters*, *409*(1), 19–23.

Fujii, M., Maesawa, S., Motomura, K., Futamura, M., Hayashi, Y., Koba, I., & Wakabayashi, T. (2015). Intraoperative subcortical mapping of a language-associated deep frontal tract connecting the superior frontal gyrus to broca's area in the dominant hemisphere of patients with glioma. *Journal of neurosurgery*, *122*(6), 1390–1396.

Geva, S., Schneider, L. M., Roberts, S., Khan, S., Gajardo-Vidal, A., Lorca-Puls, D. L., Hope, T. M., Green, D. W., Price, C. J., et al. (2021). Right cerebral motor areas that support accurate speech production following damage to cerebellar speech areas. *NeuroImage: Clinical*, *32*, 102820.

Ghosh, S. S., Tourville, J. A., & Guenther, F. H. (2008). A neuroimaging study of premotor lateralization and cerebellar involvement in the production of phonemes and syllables.

Glover, G., & Pelc, N. (2019). Method for correcting image distortion due to gradient nonuniformity. 1986. *Google Patents*.

Graziano, P. A., Garic, D., & Dick, A. S. (2022). Individual differences in white matter of the uncinate fasciculus and inferior fronto-occipital fasciculus: Possible early biomarkers for callous-unemotional behaviors in young children with disruptive behavior problems. *Journal of Child Psychology and Psychiatry*, *63*(1), 19–33.

Guenther, F. H. (2016). *Neural control of speech*. Mit Press.

Hagler Jr, D. J., Hatton, S., Cornejo, M. D., Makowski, C., Fair, D. A., Dick, A. S., Sutherland, M. T., Casey, B., Barch, D. M., & Harms, M. P. (2019). Image processing and analysis methods for the adolescent brain cognitive development study. *Neuroimage*, *202*, 116091.

Hertrich, I., Dietrich, S., & Ackermann, H. (2016). The role of the supplementary motor area for speech and language processing. *Neuroscience Biobehavioral Reviews*, *68*, 602–610.

Hickok, G., Venezia, J., & Teghipco, A. (2023). Beyond broca: Neural architecture and evolution of a dual motor speech coordination system. *Brain*, *146*(5), 1775–1790. https://doi.org/10.1093/brain/awac454

Hickok, G., Buchsbaum, B., Humphries, C., & Muftuler, T. (2003). Auditory–motor interaction revealed by fmri: Speech, music, and working memory in area spt. *Journal of cognitive neuroscience*, *15*(5), 673–682.

Hickok, G., & Poeppel, D. (2000). Towards a functional neuroanatomy of speech perception. *Trends in cognitive sciences*, *4*(4), 131–138.

Hickok, G., & Poeppel, D. (2004). Dorsal and ventral streams: A framework for understanding aspects of the functional anatomy of language. *Cognition*, *92*(1-2), 67–99.

Hickok, G., & Poeppel, D. (2007). The cortical organization of speech processing. *Nature reviews neuroscience*, *8*(5), 393–402.

Holland, D., Kuperman, J. M., & Dale, A. M. (2010). Efficient correction of inhomogeneous static magnetic field-induced distortion in echo planar imaging. *Neuroimage*, *50*(1), 175–183.

Holland, S. K., Plante, E., Byars, A. W., Strawsburg, R. H., Schmithorst, V. J., & Ball Jr, W. S. (2001). Normal fmri brain activation patterns in children performing a verb generation task. *Neuroimage*, *14*(4), 837–843.

Humphries, T., Koltun, H., Malone, M., & Roberts, W. (1994). Teacher-identified oral language difficulties among boys with attention problems. *Journal of Developmental Behavioral Pediatrics*, *15*(2), 92–98.

Irfanoglu, M. O., Modi, P., Nayak, A., Hutchinson, E. B., Sarlls, J., & Pierpaoli, C. (2015). Dr-buddi (diffeomorphic registration for blip-up blip-down diffusion imaging) method for correcting echo planar imaging distortions. *Neuroimage*, *106*, 284–299.

Jobson, K. R., Hoffman, L. J., Metoki, A., Popal, H., Dick, A. S., Reilly, J., & Olson, I. R. (2022). Language and the cerebellum: Structural connectivity to the eloquent brain. *Neurobiology of Language*. https://doi.org/https://doi.org/10.1162/nol_a_00085

Johnson, C. A., Liu, Y., Waller, N., & Chang, S.-E. (2022). Tract profiles of the cerebellar peduncles in children who stutter. *Brain Structure and Function*, *227*(5), 1773–1787.

Jossinger, S., Kronfeld-Duenias, V., Zislis, A., Amir, O., & Ben-Shachar, M. (2021). Speech rate association with cerebellar white-matter diffusivity in adults with persistent developmental stuttering. *Brain Structure and Function*, *226*, 801–816.

Jossinger, S., Yablonski, M., Amir, O., & Ben-Shachar, M. (2023). The contributions of the cerebellar peduncles and the frontal aslant tract in mediating speech fluency. *Neurobiology of Language*, 1–25.

Kemerdere, R., de Champfleur, N. M., Deverdun, J., Cochereau, J., Moritz-Gasser, S., Herbet, G., & Duffau, H. (2016). Role of the left frontal aslant tract in stuttering: A brain stimulation and tractographic study. *Journal of neurology*, *263*, 157–167.

Kinoshita, M., de Champfleur, N. M., Deverdun, J., Moritz-Gasser, S., Herbet, G., & Duffau, H. (2015). Role of fronto-striatal tract and frontal aslant tract in movement and speech: An axonal mapping study. *Brain Structure and Function*, *220*, 3399–3412.

Kronfeld-Duenias, V., Amir, O., Ezrati-Vinacour, R., Civier, O., & Ben-Shachar, M. (2016). The frontal aslant tract underlies speech fluency in persistent developmental stuttering. *Brain Structure and Function*, *221*, 365–381.

Levelt, W. J., Roelofs, A., & Meyer, A. S. (1999). A theory of lexical access in speech production. *Behavioral and brain sciences*, *22*(1), 1–38.

Lu, J., Zhao, Z., Zhang, J., Wu, B., Zhu, Y., Chang, E. F., Wu, J., Duffau, H., & Berger, M. S. (2021). Functional maps of direct electrical stimulation-induced speech arrest and anomia: A multicentre retrospective study. *Brain*, *144*(8), 2541–2553.

Mandelli, M. L., Caverzasi, E., Binney, R. J., Henry, M. L., Lobach, I., Block, N., Amirbekian, B., Dronkers, N., Miller, B. L., & Henry, R. G. (2014). Frontal white matter tracts sustaining speech production in primary progressive aphasia. *Journal of Neuroscience*, *34*(29), 9754–9767.

McGrath, L. M., Hutaff-Lee, C., Scott, A., Boada, R., Shriberg, L. D., & Pennington, B. F. (2008). Children with comorbid speech sound disorder and specific language impairment are at increased risk for attention-deficit/hyperactivity disorder. *Journal of abnormal child psychology*, *36*, 151–163.

Misaghi, E., Zhang, Z., Gracco, V. L., Luc, F., & Beal, D. S. (2018). White matter tractography of the neural network for speech-motor control in children who stutter. *Neuroscience letters*, *668*, 37–42.

Morgan, A., Liégeois, F., Liederkerke, C., Vogel, A., Hayward, R., Harkness, W., Chong, K., & Vargha-Khadem, F. (2011). Role of cerebellum in fine speech control in childhood: Persistent dysarthria after surgical treatment for posterior fossa tumour. *Brain and language*, *117*(2), 69–76.

Morgan, P. S., Bowtell, R. W., McIntyre, D. J., & Worthington, B. S. (2004). Correction of spatial distortion in epi due to inhomogeneous static magnetic fields using the reversed gradient method. *Journal of Magnetic Resonance Imaging: An Official Journal of the International Society for Magnetic Resonance in Medicine*, *19*(4), 499–507.

Muncy, N. M., Kimbler, A., Hedges-Muncy, A. M., McMakin, D. L., & Mattfeld, A. T. (2022). General additive models address statistical issues in diffusion mri: An example with clinically anxious adolescents. *NeuroImage: Clinical*, *33*, 102937.

Nagahama, H., Wanibuchi, M., Hirano, T., Nakanishi, M., & Takashima, H. (2021). Visualization of cerebellar peduncles using diffusion tensor imaging. *Acta Neurochirurgica*, *163*, 619–624.

Naidich, T. P., Duvernoy, H. M., Delman, B. N., Sorensen, A. G., Kollias, S. S., & Haacke, E. M. (2009). *Duvernoy's atlas of the human brain stem and cerebellum: High-field mri, surface anatomy, internal structure, vascularization and 3 d sectional anatomy*. Springer Science & Business Media.

Oberhuber, M., Hope, T., Seghier, M. L., Parker Jones, O., Prejawa, S., Green, D. W., & Price, C. J. (2016). Four functionally distinct regions in the left supramarginal gyrus support word processing. *Cerebral Cortex*, *26*(11), 4212–4226.

Oldfield, R. (1971). Edinburgh handedness inventory. *Journal of Abnormal Psychology*.

Olulade, O. A., Seydell-Greenwald, A., Chambers, C. E., Turkeltaub, P. E., Dromerick, A. W., Berl, M. M., Gaillard, W. D., & Newport, E. L. (2020). The neural basis of language development: Changes in lateralization over age. *Proceedings of the National Academy of Sciences*, *117*(38), 23477–23483.

Packman, A., Onslow, M., Lagopoulos, J., Shan, Z. Y., Lowe, R., Jones, M., O'Brian, S., & Sommer, M. (2022). White matter connectivity in neonates at risk of stuttering: Preliminary data. *Neuroscience letters*, *781*, 136655.

Palmer, C. E., Pecheva, D., Iversen, J. R., Hagler Jr, D. J., Sugrue, L., Nedelec, P., Fan, C. C., Thompson, W. K., Jernigan, T. L., & Dale, A. M. (2022a). Microstructural development from 9 to 14 years: Evidence from the abcd study. *Developmental cognitive neuroscience*, *53*, 101044.

Palmer, C. E., Pecheva, D., Iversen, J. R., Hagler Jr, D. J., Sugrue, L., Nedelec, P., Fan, C. C., Thompson, W. K., Jernigan, T. L., & Dale, A. M. (2022b). Microstructural development from 9 to 14 years: Evidence from the abcd study. *Developmental cognitive neuroscience*, *53*, 101044.

Parekh, P., Fan, C. C., Frei, O., Palmer, C. E., Smith, D. M., Makowski, C., Iversen, J. R., Pecheva, D., Holland, D., & Loughnan, R. (2024). *Fema: Fast and efficient mixed-effects algorithm for large sample whole-brain imaging data* (Report No. 1065-9471). Wiley Online Library.

Peeva, M. G., Guenther, F. H., Tourville, J. A., Nieto-Castanon, A., Anton, J.-L., Nazarian, B., & Alario, F.-X. (2010). Distinct representations of phonemes, syllables, and supra-syllabic sequences in the speech production network. *Neuroimage*, *50*(2), 626–638.

Rauschecker, J. P. (1998). Cortical processing of complex sounds. *Current opinion in neurobiology*, *8*(4), 516–521.

Rauschecker, J. P., & Scott, S. K. (2009). Maps and streams in the auditory cortex: Nonhuman primates illuminate human speech processing. *Nature neuroscience*, *12*(6), 718–724.

Riecker, A., Kassubek, J., Gröschel, K., Grodd, W., & Ackermann, H. (2006). The cerebral control of speech tempo: Opposite relationship between speaking rate and bold signal changes at striatal and cerebellar structures. *NeuroImage*, *29*(1), 46–53.

Riecker, A., Mathiak, K., Wildgruber, D., Erb, M., Hertrich, I., Grodd, W., & Ackermann, H. (2005). Fmri reveals two distinct cerebral networks subserving speech motor control. *Neurology*, *64*(4), 700–706.

Rvachew, S., & Matthews, T. (2017). Using the syllable repetition task to reveal underlying speech processes in childhood apraxia of speech: A tutorial. *Canadian Journal of Speech-Language Pathology & Audiology*, *41*.

Schilling, K. G., Blaber, J., Hansen, C., Cai, L., Rogers, B., Anderson, A. W., Smith, S., Kanakaraj, P., Rex, T., Resnick, S. M., Shafer, A. T., Cutting, L. E., Woodward, N., Zald, D., & Landman, B. A. (2020). Distortion correction of diffusion weighted mri without reverse phase-encoding scans or field-maps. *PLoS One*, *15*(7), e0236418. https://doi.org/10.1371/journal.pone.0236418

Schilling, K. G., Blaber, J., Huo, Y., Newton, A., Hansen, C., Nath, V., Shafer, A. T., Williams, O., Resnick, S. M., Rogers, B., Anderson, A. W., & Landman, B. A. (2019). Synthesized b0 for diffusion distortion correction (synb0-disco). *Magn Reson Imaging*, *64*, 62–70. https://doi.org/10.1016/j.mri.2019.05.008

Schlösser, R., Hutchinson, M., Joseffer, S., Rusinek, H., Saarimaki, A., Stevenson, J., Dewey, S., & Brodie, J. D. (1998). Functional magnetic resonance imaging of human brain activity in a verbal fluency task. *Journal of Neurology, Neurosurgery Psychiatry*, *64*(4), 492–498.

Schweizer, T. A., Alexander, M. P., Gillingham, S., Cusimano, M., & Stuss, D. T. (2010). Lateralized cerebellar contributions to word generation: A phonemic and semantic fluency study. *Behavioural neurology*, *23*(1-2), 31–37.

Shaffer, D., Fisher, P., Lucas, C. P., Dulcan, M. K., & Schwab-Stone, M. E. (2000). Nimh diagnostic interview schedule for children version iv (nimh disc-iv): Description, differences from previous versions, and reliability of some common diagnoses. *Journal of the American Academy of Child Adolescent Psychiatry*, *39*(1), 28–38.

Shriberg, L. D., & Lohmeier, H. L. (2008). The syllable repetition task (srt). *Phonology Project, Waisman Center, University of Wisconsin-Madison, WI, USA*.

Shriberg, L. D., Lohmeier, H. L., Campbell, T. F., Dollaghan, C. A., Green, J. R., & Moore, C. A. (2009). A nonword repetition task for speakers with misarticulations: The syllable repetition task (srt).

Shuster, L. I., & Lemieux, S. K. (2005). An fmri investigation of covertly and overtly produced mono-and multisyllabic words. *Brain and language*, *93*(1), 20–31.

Stoodley, C. J., Valera, E. M., & Schmahmann, J. D. (2012). Functional topography of the cerebellum for motor and cognitive tasks: An fmri study. *Neuroimage*, *59*(2), 1560–1570.

Taylor, E. (1991). Sandberg; s./thorley, g./giles; s.(1991): The epidemiology of childhood hyperactivity. maudsley monographs; nr. 33.

Tisdall, M. D., Hess, A. T., Reuter, M., Meintjes, E. M., Fischl, B., & van der Kouwe, A. J. (2012). Volumetric navigators for prospective motion correction and selective reacquisition in neuroanatomical mri. *Magnetic resonance in medicine*, *68*(2), 389–399.

Tremblay, P., & Dick, A. S. (2016). Broca and wernicke are dead, or moving past the classic model of language neurobiology. *Brain and language*, *162*, 60–71.

Tremblay, P., & Gracco, V. L. (2009). Contribution of the pre-sma to the production of words and non-speech oral motor gestures, as revealed by repetitive transcranial magnetic stimulation (rtms). *Brain research*, *1268*, 112–124.

Tremblay, P., & Gracco, V. L. (2010). On the selection of words and oral motor responses: Evidence of a response-independent fronto-parietal network. *Cortex*, *46*(1), 15–28.

Turkeltaub, P. E., Eden, G. F., Jones, K. M., & Zeffiro, T. A. (2002). Meta-analysis of the functional neuroanatomy of single-word reading: Method and validation. *Neuroimage*, *16*(3), 765–780.

Urban, P. P., Marx, J., Hunsche, S., Gawehn, J., Vucurevic, G., Wicht, S., Massinger, C., Stoeter, P., & Hopf, H. C. (2003). Cerebellar speech representation: Lesion topography in dysarthria as derived from cerebellar ischemia and functional magnetic resonance imaging. *Archives of neurology*, *60*(7), 965–972.

Vassal, F., Boutet, C., Lemaire, J.-J., & Nuti, C. (2014). New insights into the functional significance of the frontal aslant tract: An anatomo–functional study using intraoperative electrical stimulations combined with diffusion tensor imaging-based fiber tracking. *British journal of neurosurgery*, *28*(5), 685–687.

Vias, C., & Dick, A. S. (2017). Cerebellar contributions to language in typical and atypical development: A review. *Developmental neuropsychology*, *42*(6), 404–421.

White, N. S., Leergaard, T. B., D'Arceuil, H., Bjaalie, J. G., & Dale, A. M. (2013a). Probing tissue microstructure with restriction spectrum imaging: Histological and theoretical validation. *Human brain mapping*, *34*(2), 327–346.

White, N. S., Leergaard, T. B., D'Arceuil, H., Bjaalie, J. G., & Dale, A. M. (2013b). Probing tissue microstructure with restriction spectrum imaging: Histological and theoretical validation. *Human brain mapping*, *34*(2), 327–346.

White, N. S., McDonald, C. R., Farid, N., Kuperman, J. M., Kesari, S., & Dale, A. M. (2013). Improved conspicuity and delineation of high-grade primary and metastatic brain tumors using "restriction spectrum imaging": Quantitative comparison with high b-value dwi and adc. *American Journal of Neuroradiology*, *34*(5), 958–964.

White, N. S., McDonald, C. R., Farid, N., Kuperman, J., Karow, D., Schenker-Ahmed, N. M., Bartsch, H., Rakow-Penner, R., Holland, D., & Shabaik, A. (2014). Diffusion-weighted imaging in cancer: Physical foundations and applications of restriction spectrum imaging. *Cancer research*, *74*(17), 4638–4652.

Willems, R. M., Özyürek, A., & Hagoort, P. (2009). Differential roles for left inferior frontal and superior temporal cortex in multimodal integration of action and language. *Neuroimage*, *47*(4), 1992–2004.

Yablonski, M., Rastle, K., Taylor, J., & Ben-Shachar, M. (2019). Structural properties of the ventral reading pathways are associated with morphological processing in adult english readers. *cortex*, *116*, 268–285.

Yeatman, J. D., Dougherty, R. F., Myall, N. J., Wandell, B. A., & Feldman, H. M. (2012). Tract profiles of white matter properties: Automating fiber-tract quantification. *PloS one*, *7*(11), e49790.

Yeatman, J. D., Dougherty, R. F., Rykhlevskaia, E., Sherbondy, A. J., Deutsch, G. K., Wandell, B. A., & Ben-Shachar, M. (2011). Anatomical properties of the arcuate fasciculus predict phonological and reading skills in children. *Journal of cognitive neuroscience*, *23*(11), 3304–3317.

Yendiki, A., Koldewyn, K., Kakunoori, S., Kanwisher, N., & Fischl, B. (2014). Spurious group differences due to head motion in a diffusion mri study. *Neuroimage*, *88*, 79–90.

Zhong, A. J., Baldo, J. V., Dronkers, N. F., & Ivanova, M. V. (2022a). The unique role of the frontal aslant tract in speech and language processing. *NeuroImage: Clinical*, *34*, 103020.

Zhong, A. J., Baldo, J. V., Dronkers, N. F., & Ivanova, M. V. (2022b). The unique role of the frontal aslant tract in speech and language processing. *NeuroImage: Clinical*, *34*, 103020.